AD-A186 075 EXPERIMENTAL INVESTIGATION OF DAMPING CHARACTERISTICS OF BOLTED STRUCTURAL CONNECTIONS FOR PLATES AND SHELLS (U) NAVAL POSTGRADUATE SCHOOL MONTEREY CA J C IVERSON SEP 87 1/1

UNCLASSIFIED F/G 13/5 NL

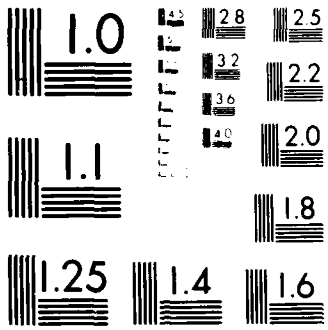

MICROCOPY RESOLUTION TEST CHART

NATIONAL BUREAU OF STANDARDS-1963-A

NAVAL POSTGRADUATE SCHOOL

Monterey, California

THESIS

EXPERIMENTAL INVESTIGATION OF DAMPING CHARACTERISTICS OF BOLTED STRUCTURAL CONNECTIONS FOR PLATES AND SHELLS

by

Jonathan C. Iverson

September 1987

Thesis Advisor: Y. S. Shin

Unclassified

SECURITY CLASSIFICATION OF THIS PAGE

REPORT DOCUMENTATION PAGE

1a. REPORT SECURITY CLASSIFICATION: UNCLASSIFIED	1b. RESTRICTIVE MARKINGS
2a. SECURITY CLASSIFICATION AUTHORITY	3. DISTRIBUTION/AVAILABILITY OF REPORT: Approved for public release; distribution is unlimited
2b. DECLASSIFICATION / DOWNGRADING SCHEDULE	
4. PERFORMING ORGANIZATION REPORT NUMBER(S)	5. MONITORING ORGANIZATION REPORT NUMBER(S)
6a. NAME OF PERFORMING ORGANIZATION: Naval Postgraduate School — 6b. OFFICE SYMBOL (If applicable): 69	7a. NAME OF MONITORING ORGANIZATION: Naval Postgraduate School
6c. ADDRESS (City, State, and ZIP Code): Monterey, California 93943-5000	7b. ADDRESS (City, State, and ZIP Code): Monterey, California 93943-5000
8a. NAME OF FUNDING/SPONSORING ORGANIZATION — 8b. OFFICE SYMBOL (If applicable)	9. PROCUREMENT INSTRUMENT IDENTIFICATION NUMBER
8c. ADDRESS (City, State, and ZIP Code)	10. SOURCE OF FUNDING NUMBERS: PROGRAM ELEMENT NO — PROJECT NO — TASK NO — WORK UNIT ACCESSION NO

11. TITLE (Include Security Classification): EXPERIMENTAL INVESTIGATION OF DAMPING CHARACTERISTICS OF BOLTED STRUCTURAL CONNECTIONS FOR PLATES AND SHELLS

12. PERSONAL AUTHOR(S): Iverson, Jonathan C.

13a. TYPE OF REPORT	13b. TIME COVERED	14. DATE OF REPORT (Year, Month, Day)	15. PAGE COUNT
Master's Thesis	FROM ____ TO ____	1987, September	[illegible]

16. SUPPLEMENTARY NOTATION

17. COSATI CODES			18. SUBJECT TERMS (Continue on reverse if necessary and identify by block number)
FIELD	GROUP	SUB-GROUP	Structural Damping, Bolted Connections, Viscoelastic Materia[l], Random Excitation, Swept Sine Excitation, Shells and Plates

19. ABSTRACT (Continue on reverse if necessary and identify by block number)

Reducing the contact force in bolted structural connections canreduce system vibration amplitudes by enhancing joint damping capacity. A test model consisting of two concentric circular cylindrical shells and four vanes connected by groups of bolts was tested and analyzed to investigate the relationship between the contact force and the system damping. A viscoelastic material was then introduced between the contacting surfaces and its effects on system damping were again investigated.

Experimental results show that resonant frequencies of modes whose mode shapes provided the most differential motion at the joint connection were

20. DISTRIBUTION/AVAILABILITY OF ABSTRACT: ☒ UNCLASSIFIED/UNLIMITED ☐ SAME AS RPT ☐ DTIC USERS	21. ABSTRACT SECURITY CLASSIFICATION: UNCLASSIFIED
22a. NAME OF RESPONSIBLE INDIVIDUAL: Professor Young S. Shin	22b. TELEPHONE (Include Area Code): (408) 646-2568 — 22c. OFFICE SYMBOL: 69SG

DD FORM 1473, 84 MAR — 83 APR edition may be used until exhausted. All other editions are obsolete.

SECURITY CLASSIFICATION OF THIS PAGE

Unclassified

Block 19 cont.

shifted down in frequency and the damping increased. This damping increase and frequency shift continued as contact force was reduced until the structural joints moved into the total slip regime where the response becomes nonlinear. The maximum damping and maximum frequency shift were obtained just prior to this total slip.

The greatest increase in damping was achieved with the introduction of viscoelastic material between contact surfaces. This damping material also postponed the transition from microslip to macroslip.

Experimental Investigation of Damping Characteristics of Bolted Structural Connections for Plates and Shells

by

Jonathan C. Iverson
Lieutenant, United States Navy
B.S., University of Miami, 1979

Submitted in partial fulfillment of the
requirements for the degrees of

MASTER OF SCIENCE IN MECHANICAL ENGINEERING

and

MECHANICAL ENGINEER

from the

NAVAL POSTGRADUATE SCHOOL
September 1987

Author: Jonathan C. Iverson
Jonathan C. Iverson

Approved by: Young S. Shin
Young S. Shin, Thesis Advisor

Kilsoo Kim
Kilsoo Kim, Second Reader

Anthony J. Healey
Anthony J. Healey, Chairman,
Department of Mechanical Engineering

G. E. Schacher
Gordon E. Schacher,
Dean of Science and Engineering

ABSTRACT

Reducing the contact force in bolted structural connections can reduce system vibration amplitudes by enhancing joint damping capacity. A test model consisting of two concentric circular cylindrical shells and four vanes connected by groups of bolts was tested and analyzed to investigate the relationship between the contact force and the system damping. A viscoelastic material was then introduced between the contacting surfaces and its effect on systems damping were again investigated.

Experimental results show that resonant frequencies of modes whose mode shapes provided the most differential motion at the joint connection were shifted down in frequency and the damping increased. This damping increase and frequency shift continued as contact force was reduced until the structural joints moved into the total slip regime where the response becomes nonlinear. The maximum damping and maximum frequency shift were obtained just prior to this total slip.

The greatest increase in damping was achieved with the introduction of viscoelastic material between contact surfaces. This damping material also postponed the transition from microslip to macroslip.

TABLE OF CONTENTS

ACKNOWLEDGEMENTS

The author would like to express his appreciation for the guidance and friendship extended by Prof. Young Shin. The technical and theoretical support for the modal analysis portion was provided by Dr. Kilsoo Kim, who made a complex subject much easier. Finally the author would like to gratefully acknowledge the continued support provided by Dr. Arthur Kilcullen and the personnel at the Naval Research and Development Center, Bethesda, Md., who funded much of the research contained in the thesis.

I. INTRODUCTION

In today's U.S. Navy design trends are tending toward lighter, all-welded structures, since a lighter structure decreases the total mass, and a welded construction configuration increases the strength of the lighter structure. This technique, however, produces structures with low inherent damping, and problems can occur under dynamic loading, which the structure could encounter during its service life. Such problems include: structural noise, critical alignment variations, dynamic stressing, and fatigue. Designs which enhance damping in a structure are, therefore, very desirable from the aspect of noise reduction and structural integrity.

Damping exists in all vibrating systems. There are many different mechanisms which contribute to the damping in a structure. Some of these mechanisms are: fluid resistance, the use of viscoelastic materials, internal friction (material damping), and friction at connections. All of these mechanisms have been shown to be a function of many variables, including a structure's shape or geometry, its material properties, temperature, frequency, boundary conditions, and different excitation energy levels.

Usually over ninety percent of the inherent damping associated with fabricated structures originates in the mechanical joints [Ref. 1]. These mechanical joints are friction joints which dissipate energy during the vibration of a structure. This vibrational damping occurs when small relative movements take place between joint interfaces. Effective use of this type of damping mechanism is very rarely utilized in the

mechanical engineering field. This is due to the current design approach of preloading all bolted joints to ninety percent of the bolting material's proof strength. This design criteria is utilized to ensure structural integrity and stiffness and to prevent interfacial slipping which would then lead to structural wear. This design approach, however, is based solely on the bolting material and not on the joint's expected excitation energy. Use of this engineering practice results in the joint damping capacity being kept to a minimum.

This investigation pursues possible damping benefits achievable by: (1) varying the contact force between joint interfaces via bolt torque adjustments, (2) damping associated with the addition of a viscoelastic layer between the friction joints contact surface, (3) a combination of both viscoelastic and varying bolt torque, to obtain an optimum joint damping, and (4) fluid loading variation by changing the structures environment from air to water. The investigation also includes the experimental verification of the macroslip phenomena at the bolted joints of the plate and shell structure.

II. BACKGROUND

Understanding of friction damping phenomena in joints has long been a significant research topic. Both analytical studies and experimental verification have pursued one of two analytical approaches, microslip or macroslip.

In the macroslip approach, the entire joint contact surfaces interfaces is assumed to be either totally stuck (no movement) or totally slipping. The frictional energy dissipation mechanism associated with the joints contact surfaces is assumed to be governed by some form of Coulomb's law of dry friction. In the microslip approach, the joint interface progressively moves from stuck to total slip, with increasing extent of local slip between pairs of contacting points. This approach produces a smoother transition from stick to total slip but requires a relatively detailed analysis of the contact stress distribution at the interface.

Macroslip analytical analysis has been conducted on both single-degree-of-freedom (SDOF) systems, and multimode systems. An exact solution for a SDOF system at steady state stick/slip motion has been obtained by Den Hartog [Ref. 2]. Figure 2.1 indicates the type of system analyzed which assumes a Coulomb friction type resisting force (F),
to the input excitation force with amplitude (P). Den Hartog's solution was limited by assuming the stick/slip motion achieve total lockup twice per cycle. His solution revealed that for forced vibration with dry friction, ratios of friction force to excitation amplitudes (F/P) of less than $^{\Pi}/4$ result in resonance response amplitudes becoming infinitely large (see

Figure 2.2). In Figure 2.2 w_R is the resonance frequency of the system. This analysis was extended to multimode systems by Pratt and Williams [Ref. 3], with similar results.

A SDOF system with bilinear hysteresis to sinusoidal excitation was analyzed by Caughy [Ref. 4]. This bilinear hysteresis behavior represented the presence of Coulomb friction or elastoplastic behavior of the system material. His analysis showed that there exists a critical value of excitation above which non-finite resonance amplitudes occur. The displacements indicated by his analysis were also larger than those obtained from an equivalent linear system model. A similar analysis of a limited slip joint to sinusoidal excitation was conducted by Iwan [Ref. 5]. This analysis revealed that the system may possess such features as large jumps and/or discontinuous response curves which depend on the severity of the non-linearity induced by slip, the level of excitation, and the amount of viscous damping.

Discrete models to characterize the dynamic responses of a bladed disk system with dry friction dampers, excited by harmonic forces was developed and examined by Muszynska and his co-workers [Ref. 6 and 7]. This model determined that two factors were highly influential on the frictional damping realized. These factors are: (a) the ratio of the friction force to the excitation force, and (b) the blade-to-blade phase angle of the exciting force. The frictional elements also introduced a coupling of the system components.

The origins of the microslip analysis can be found historically in Mindlin's extension of Hertz's contact analysis between two spheres. The major application of microslip analysis on friction damping in joints can be found in contact analysis between flat surfaces.

The energy dissipation at an axial double lapped joint under partial slip and then gross slip was analyzed by Earles and Philpot [Ref. 8]. This analysis indicated that the energy dissipated was proportional to the cube of the load and inversely proportional to the coefficient of friction for the partial slip case. Their experiments were conducted on plain stainless steel flat plates with the frictional damping occurring under oscillating tangential loads. They obtained a close agreement for the partial slip region obtained previously by analytical means.

Most recent applications of this dry friction damping analysis have been applied to space structures in which a truss structure is made of tubular members. Crawley et. al. [Ref. 9] considered a friction damping mechanism consisting of segmented damping tubes placed end to end inside the tubular load carrying members. A simple mircoslip Coulomb type friction model was analyzed to determine the energy loss per cycle and then validated on a one dimensional friction damping model. The resulting curves showed close agreement between theory and experiments.

Menq, Griffin and Bielak [Ref. 10] developed a microslip model which allowed partial slip on the contact interface. The model consisted of two elastic bars joined by an elastoplastic shear layer as shown in Figure 2.3. The friction force in the shear layer, τ, per unit length is given by,

$$\tau = \begin{cases} k\mu, & |\mu| < \tau_m / k \\ \tau_m, & \text{otherwise} \end{cases}$$

where τ_m is the maximum shear stress for the occurrence of local plastic deformation. The system will deform elastically as the displacement at the end of the bar

remains below the value τ_m/k. As the load P increases beyond this value a region of slip is generated and this region increases until the entire shear layer becomes plastic.

This microslip model was used to simulate the vibration response of three sets of experiments [Ref. 11]. In each case the microslip model could explain the experimental results that could not be explained by the macroslip model. Figure 2.4 displays the actual experimental response obtained for a beam with platform arrangement. Figure 2.5 shows the results obtained utilizing the numerical macroslip model and Figure 2.6 illustrates the close agreement obtained from the microslip model.

Beards and Williams [Ref. 12] constructed a test frame consists of a rectangular frame with a solid steel bar bolted diagonally to it. The frequency response of the structure was measured by exciting one corner of the frame at a constant sinusoidal force and detecting the response by an accelerometer at one of the other corners of the frame. They analyzed the response of the frame using a method that analyzes the vibration of a system, which is comprised of a linear undamped multi-degree-of-freedom structure with a single frictional damper [Ref. 13]. This experiment indicated that a useful increase in the damping in a structure could be achieved by fastening joints tightly to prohibit translational slip but not tightly enough to prohibit rotational slip.

An investigation of the effect of controlled friction damping in joints on the frequency response of a frame excited by a harmonic force was preformed by Beards and Woodwat [Ref. 1]. They compared the frequency response around the second mode of vibration of the frame for various clamping forces at the joints.

It was observed that a maximum reduction in the frame's response of 21 dB could be achieved. It was also shown that a reduction in peak response of 10 dB occurred due only to microslip in the joints.

Vibration damping associated with dry friction in turbine engines can occur at shroud interfaces of blades and the platform of turbine blades fitted with platform dampers. Srinivasan and Cutts [Ref. 14] studied the effect of these two sources of damping on blade vibration both experimentally and analytically. In the study of damping due to rubbing at shroud interfaces, the macroslip analysis predicted an abrupt transition from a region of no friction damping to the macroslip region. However, the test results indicated a smoother transition indicating a region of partial slip or microslip conditions.

From all of these research papers and experiments, it is clear that the macroslip model is not enough to obtain an understanding of the damping associated with clamping forces. It is also clear that the excitation force defines the region as micro or macroslip and that the current trend in the analytical approach should be the development of a new model which exhibits the three main characteristics of such contact problems. These characteristics are: elastic deformation at small excitation energies, followed by a region of partial or microslip, and finally a total slipping of the joint for very large excitation forces.

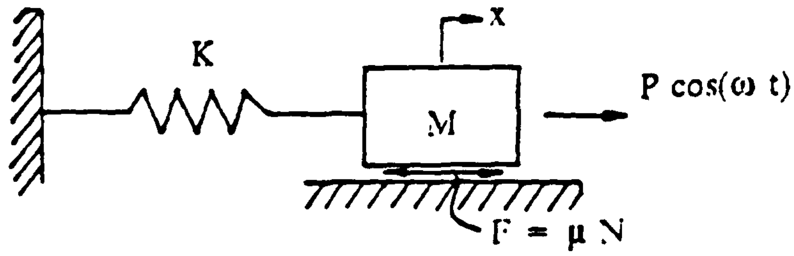

Figure 2.1 Single degree-of-freedom system with Coulomb friction.

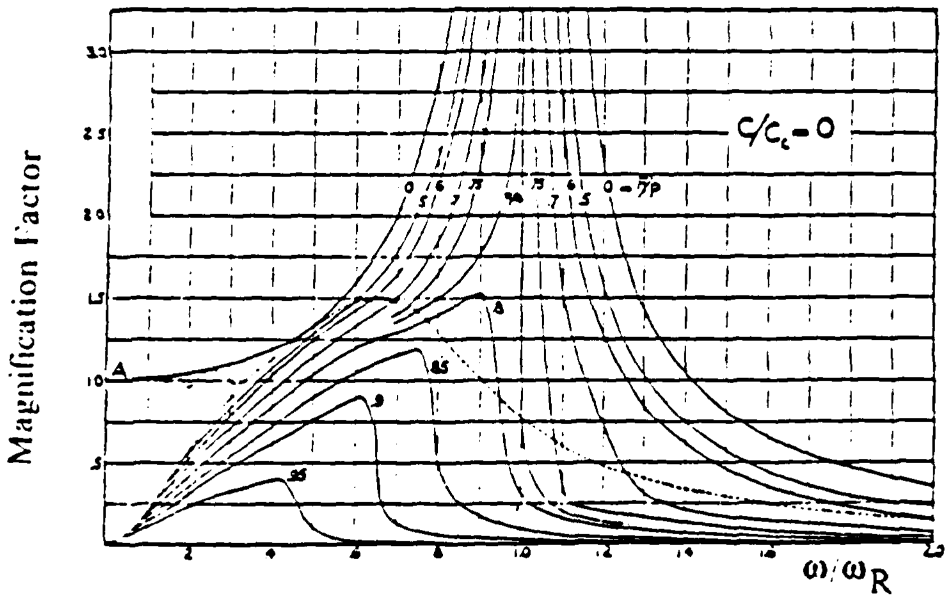

Figure 2.2 Forced vibration with friction damping only. [Ref. 2]

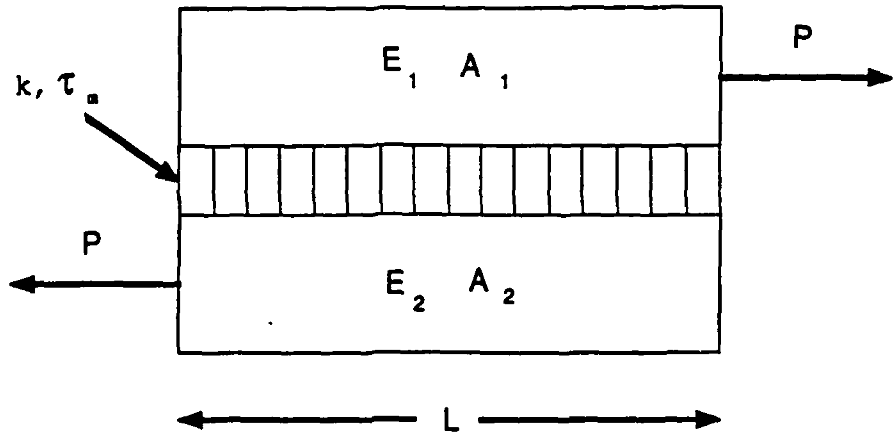

Figure 2.3 Microslip model with elastoplastic shear layer.

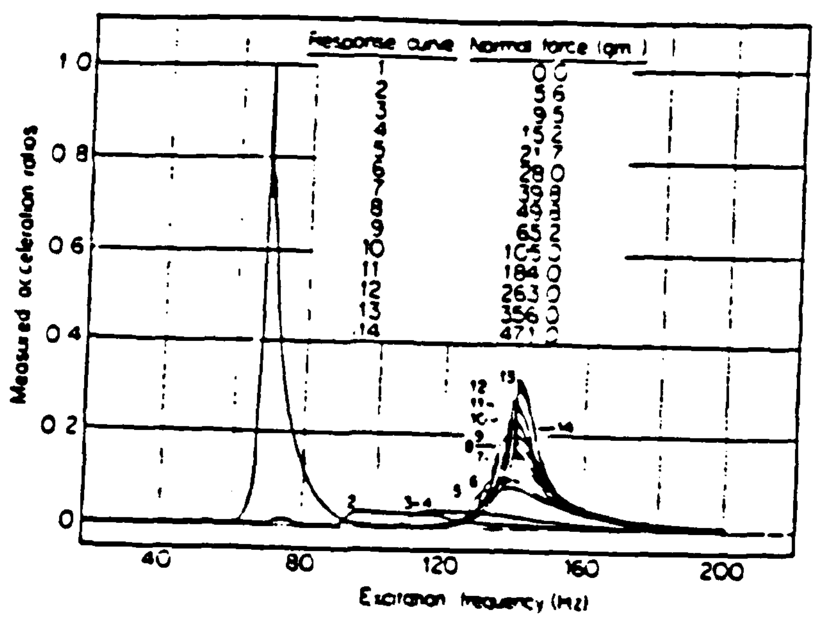

Figure 2.4 Vibration response of a beam with platform. [Ref. 11]

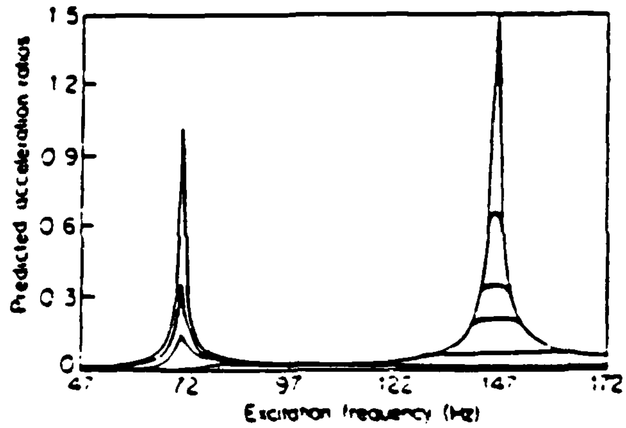

Figure 2.5 Response predicted by macroslip friction model. [Ref. 11]

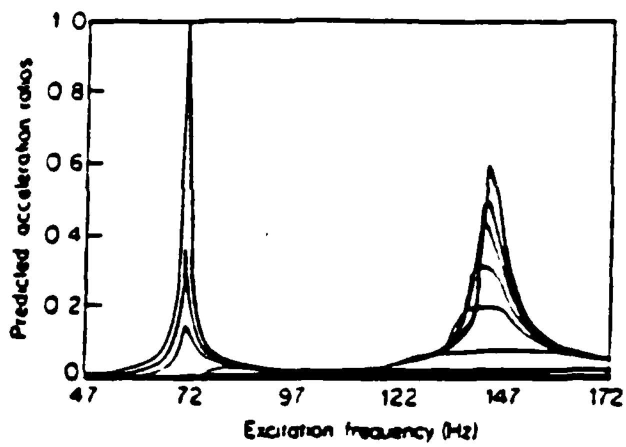

Figure 2.6 Response predicted by microslip friction model. [Ref. 11]

III. THEORY AND METHOD

One of the important concepts in signal processing is that of developing a clear understanding of time-frequency and Laplace domain transformations. These transformations simply transform either data or expressions from one in-dependent variable to another. The variables are time (t), frequency (w), or the Laplace operator (s).

The transformation process generates no new information but simply puts the data in a form which is more easily interpretable or computationally simpler.

In this thesis work these transformations were used extensively in the analysis of the data obtained. Fourier Transforms were used for computing frequency response and coherence functions.

The frequency response of a system is defined as the Fourier transform of the input to the system divided into the Fourier transform of the output of the system, or:

$$H(jw) = O(jw) / I(jw)$$

where $H(jw)$ = frequency response
$O(jw)$ = Fourier transform of output
$I(jw)$ = Fourier transform of input.

The transfer function is defined as the Laplace transform of the system output divided by the Laplace transform of the system input, or:

$$G(s) = O(s) / I(s)$$

where $G(s)$ = transfer function
$O(s)$ = Laplace transform of output

$I(s)$ = Laplace transform of input.

The frequency response and transfer function supply essentially the same information about the system. The two terms are frequently used interchangeably in the literature. The frequency response of a system is determined from the transfer function by letting $s = jw$ and by assuming that all initial disturbances were either equal to zero or completely damped.

In the majority of present day vibrational analysis, the motion of the physical system is assumed to be adequately described by a set of simultaneous second-order linear differential equations of the form:

$$M\ddot{x}(t) + C\dot{x}(t) + Kx(t) = f(t) \qquad \text{equ 3.1}$$

where $f(t)$ is the applied force vector, $x(t)$, $\dot{x}(t)$, and $\ddot{x}(t)$ are the resulting displacement, velocity, and acceleration vectors, and M, C, and K are called the mass, damping, and stiffness matrices. If the system has n-dimensions (n-degrees-of-freedom) then the above vectors are n-dimensional and the matrices are $(n \times n)$.

Taking the Laplace transform of the system gives:

$$B(s) * X(s) = F(s) \qquad \text{equ 3.2}$$

where $F(s)$ is the Laplace transform of applied force vector, $X(s)$ is the Laplace transform of resulting displacement vector, $B(s) = Ms^2 + Cs + K$, and s is the Laplace variable, a complex number. $B(s)$ is referred to as the system matrix. The transfer matrix $H(s)$ is defined as the inverse of the system matrix. Hence, the transfer matrix $H(s)$ satisfies the following equation:

$$X(s) = H(s) * F(s)$$

which is equivalent to equation 3.2.

This investigation assumes that the responses of the model associated with microslip are linear in nature. With this assumption it is possible to describe the motion of the system as described above in equation 3.1.

The frequency response can be determined by substitution of jw for s in the transfer function or is also define as:

$$H(\omega) = \frac{1/m}{\sqrt{(\omega_n^2 - \omega^2) + (2\zeta\omega\omega_n)^2}}$$

where

$$\omega_n^2 = \frac{k}{m} \quad , \; 2\zeta\omega_n = \frac{c}{m} \quad , \text{ or } \zeta = \frac{c}{\sqrt{2km}}$$

This result is for the single-degree-of-freedom system but is a simplification of the multi-degree system solution.

The frequency response is a complex quantity and contains both real and imaginary parts (rectangular coordinates). It can also be presented in a polar coordinates as magnitude and phase. Both systems provide the same information, however, the dB scaled transfer function or Bode plot provides the most information in one graphical presentation and used in this paper.

Modal Analysis is a method by which the dynamic properties of a system (damping, natural frequency, and mode shape) can be determined. There are three fundamental assumptions concerning the nature of the system upon which modal analysis is based. These assumptions are:

1. The system is linear. The response of the

structure to a combination of forces, simultaneously applied, is the sum of the individual responses to each of the forces acting alone.

2. The structure is time-invariant or "stationary". The measured modal parameters are constants of the system.
3. The structure is observable. The force input and acceleration output measurements taken contain enough information to generate an adequate behavioral model.

The damping and frequency associated with a particular mode of vibration are global properties of the structure under test and theoretically independent of where they are measured on the structure (assuming the measurement is not performed at a nodal point). The mode shapes are a spatial description of the elastic response of the structure and also influenced by node point locations. To determine a mode shape requires that sufficient measurements be taken such that when the modal analysis is preformed and the mode shape calculated the individual mode shapes accurately describe the dynamic motion of the system under test.

A more detailed description of both modal analysis and transfer function are contain in References 15 and 16.

IV. EXPERIMENTAL ARRANGEMENT

A. MODEL CONSTRUCTION

A test model was constructed which consisted of two concentric cylindrical shells with a four vane intra-structure. All connections were by bolts, as shown in Figure 4.1. The outer shell was made of a standard carbon steel, 0.25 inches in thickness and 18.0 inches wide. The remaining structural material was bronze which was also 0.25 inches thick and 18.0 inches wide (see Figure 4.1). Note that the inner shell is 0.5 inches thick. High strength A325 bolts 0.75 inches in diameter and double washers were utilized throughout the structure to connect all structural pieces together. Bolts were arranged in groups of six, uniformly spaced per row, each row being located on bolt lines as shown in Figure 4.1. Bolting hole were tapped such that the bolts had a 0.125 inch clearance and were not in direct contact with the structure. This provided the bolts the ability to move relative to the structure, which is similar to the standard engineering application. The other connections at the vane plates to support structures were full penetration welds.

Maximum contact force was determined utilizing a typical machine design calculation:

$$Fi = 0.9 * Sp * At$$

where Fi is the proof load or contact force for each bolt, Sp is the proof strength of the bolt material, and At is the tensile-stress area. This result can quickly be modified to obtain bolt torque by:

$$T = 0.2 * Fi * D$$

where T is the torque for each bolt and D is the

diameter of the bolt. Values obtained for maximum torque and contact force were 320.0 ft-lb and 3.06×10^6 lb. For the continuation of the study all torques and contact forces were taken as percentages of these maximum values.

Previous studies conducted at the Naval Postgraduate School have concluded that the optimum boundary condition is that of shock chord induced free-free support [Ref. 17]. This type of support was utilized for the study and was found to limit the transmission of random noise signals from the local environment to the structure.

B. IMPACT TESTING ARRANGEMENT

Two different approaches were taken to determine the best process in which to investigate the model's response. The first was an impact-decay type analysis (see Figure 4.2), in which a PCB modally tuned impact hammer was used to excite the model and a miniature ENDEVCO accelerometer (model 2250A10) measured the structures response. Each of 96 grid points was excited ten times and averaged to obtain input and output signals. These input and output signals were amplified and filtered prior to analysis. The input signal was obtained from a force transducer located in the head of the impact hammer. This signal was then amplified by a PCB Power unit (model 480D06) with the gain value set at ten. The response signal was amplified by an ENDEVCO signal conditioner (model 4416A), which was also set with a gain factor of ten. These two signals were both pre-filtered by a Hewlett Packard (HP) 5440A Low Pass Filter and analyzed by a HP 5451C Fourier Analyzer.

The HP 5451C Fourier Analyzer utilizes a band-selectable Fourier analysis technique that makes it

possible to perform Fourier analysis over a frequency band whose upper and lower frequencies are independently selectable. It also provides a digital frequency domain analysis of complicated time signals. A modal analysis application package operates on measured transfer function data to determine modal properties, this includes an animation of the particular mode shape. From this analysis the first eight mode shapes were determined.

C. VIBRATION GENERATOR TESTING ARRANGEMENT

The second process (see Figure 4.3) employed a Wilcoxon Research F7/F4 Vibration Generator as the input force device. The vibration generator was attached to one of the vanes on the structure, 5.5 inches from the outside shell and six inches from the front edge of the vane. This vibration generator utilizes a combination electromechanical and piezoelectric units which provide a controllable force output in the range of 10 Hz to 15,000 Hz. An HP 3562A Dynamic Signal Analyzer provided the driving signal which was amplified by a Wilcoxon Research Power Amplifier (model PA7C). The driving signal was either a frequency selected random noise or a swept sine. This amplified signal was then properly split into two signals by a Wilcoxon Matching Network (model PA7C). The split is determined by the frequency of the driving signal. The lower the desired frequency the more power is provided to the electromechanical (F7) vibration generator. Similarly, when the high frequency signal is desired, power is sent to the piezoelectric (F4) vibration generator. This separation is to ensure a smooth transition from low frequency to the higher ranges. Located at the base of this vibration generator and before the attachment post was a force

transducer to measure the input excitation force. This force signal was then amplified by a charge amplifier and fed to the HP 3562A Dynamic Signal Analyzer as an input signal. An ENDEVCO accelerometer and signal conditioner were used to measure the structure's response. This signal was also fed to the HP 3562A Analyzer as the output signal. When the input signal was random noise the output signal was subjected to a Hanning window and utilized a 40 averaging analysis. Then the swept sine is utilized there is no requirement for windowing, however a ten averaging analysis was taken. The accelerometer was placed in ten different grid points, symmetrically oriented about the center of the structure. These grid points were both on the outer shell as well as the vane structures.

The HP 3562A Dynamic Signal Analyzer digitized both input and output signals, from this digitized data the analyzer calculates frequency response, power spectra, and coherence. Coherence shows the relative reliability of the data obtained. Its range is from 1.0 to 0.0, or from exact data, to data fully contaminated by noise.

For the underwater experimentation, a waterproof case was utilized. The case was previously designed, constructed and tested at the Naval Postgraduate School. More information as to the construction and checkout testing can be obtained from Reference 18.

D. VISCOELASTIC MATERIAL

The viscoelastic material applied at the joint interfaces was a 3M SJ-2015x ISD-112 viscoelastic compound. This material was conveniently provided as thin sheets, approximately 10 mil. in thickness. Figure 4.4 shows the variation of the shear modulus and loss factor as functions of temperature and frequency

for the ISD-112 viscoelastic material alone. These plots are usually used for the design of constrained layer dampers. The stiffness, mass, resonance mode configuration, and geometry of the damper-substrate combination significantly affects the performance of the viscoelastic material. The ISD-112 viscoelastic material was selected because of it's consistent loss factor over a wide range of temperatures. This can be seen in Figure 4.4, that the loss factor is relatively flat from 100 F to 50 F. The modulus of elasticity changes significantly but this is characteristic of all viscoelastic materials.

E. GENERAL TEST PLAN

The experimentation was broken down into four areas. First a modal analysis was conducted to determine the structures modes shapes and resonance frequencies. Next a verification study to ensure repeatability of the structural response and optimum test equipment arrangements. The third area studied was the effects on structural damping associated with the model by varying the contact force. The final examination was to observe the effects of a viscoelastic joint and varying contact force.

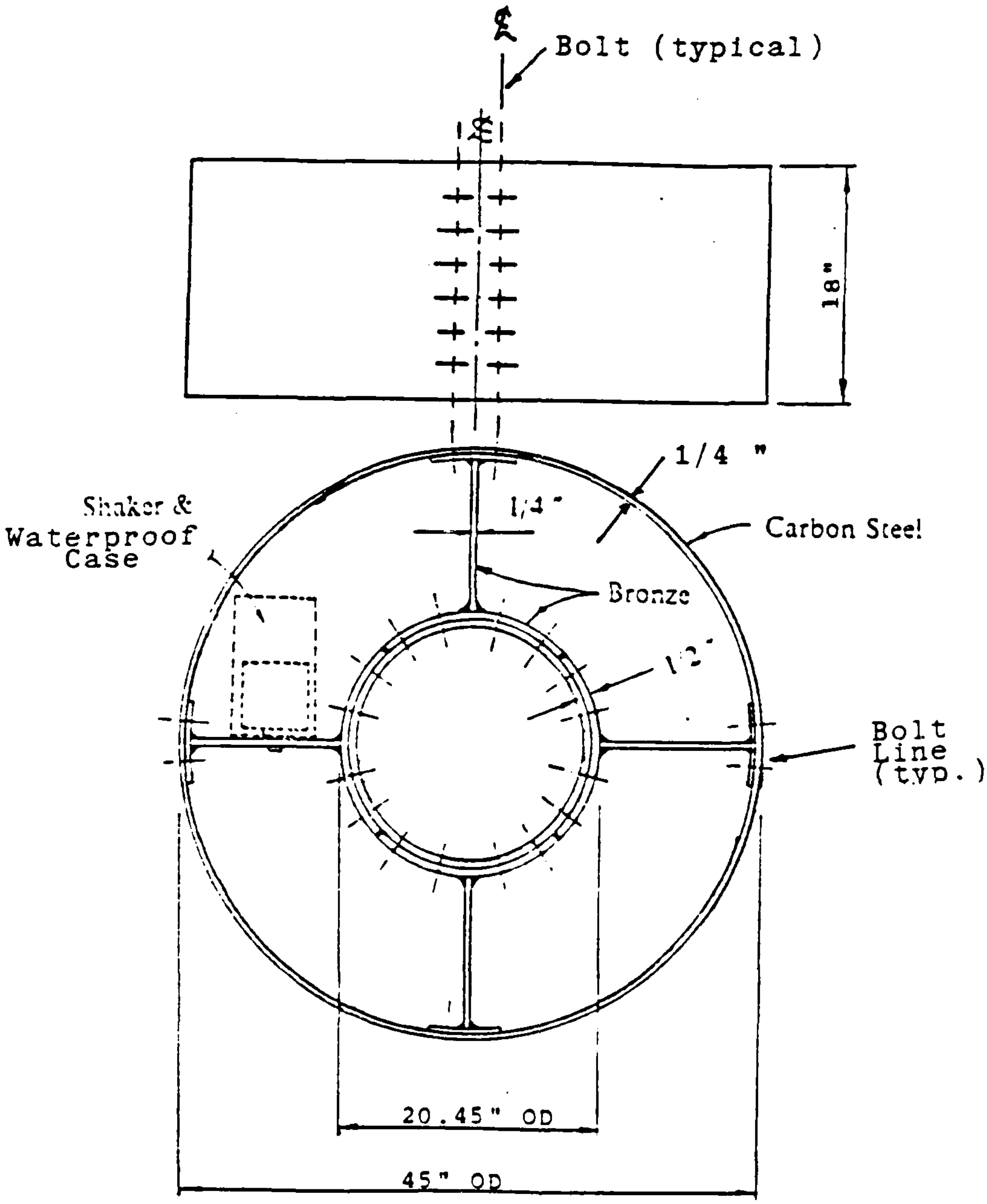

(NOTE: each bolt line has six bolts in uniform spacing)
Figure 4.1 Structural Dimensions of the Test Model.

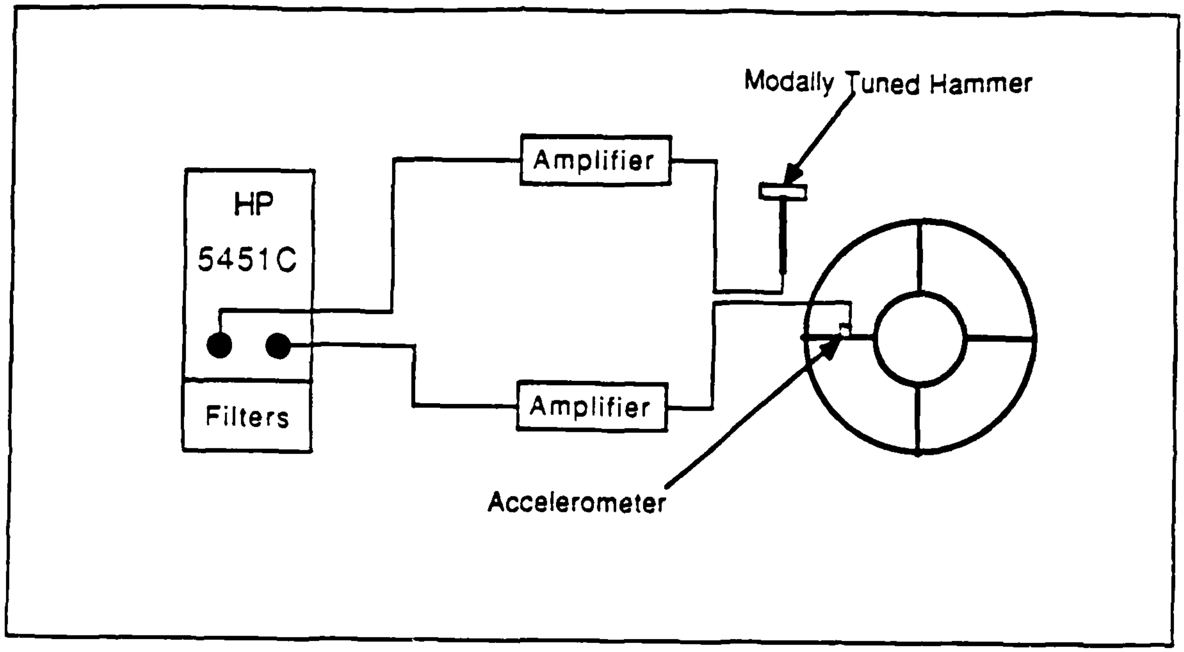

Figure 4.2 Impact-response type experimental arrangement.

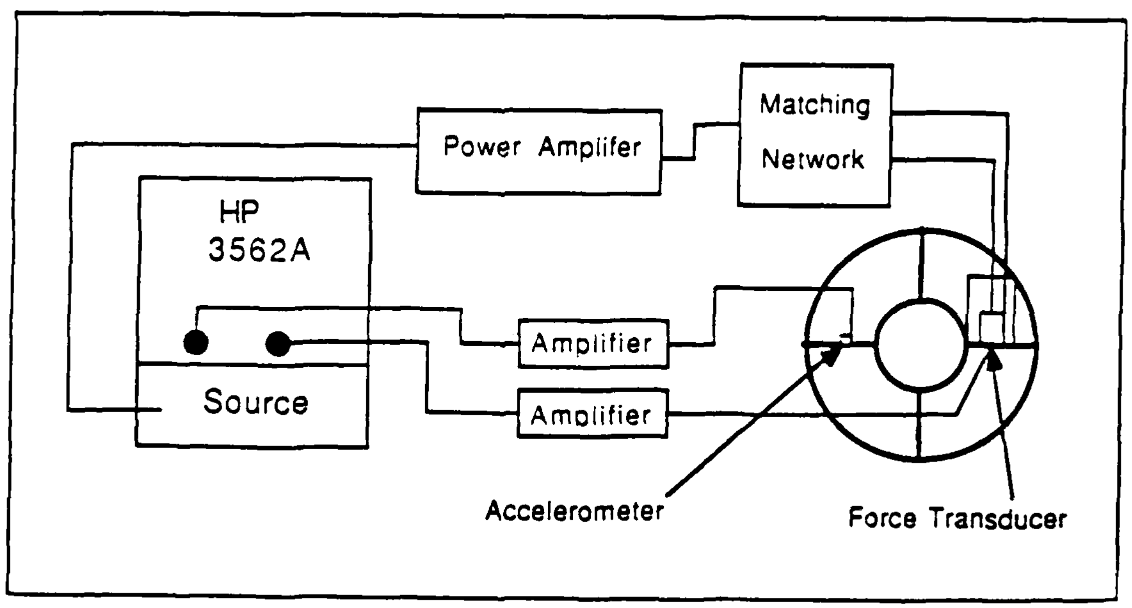

Figure 4.3 Vibration generator and response, experimental arrangement.

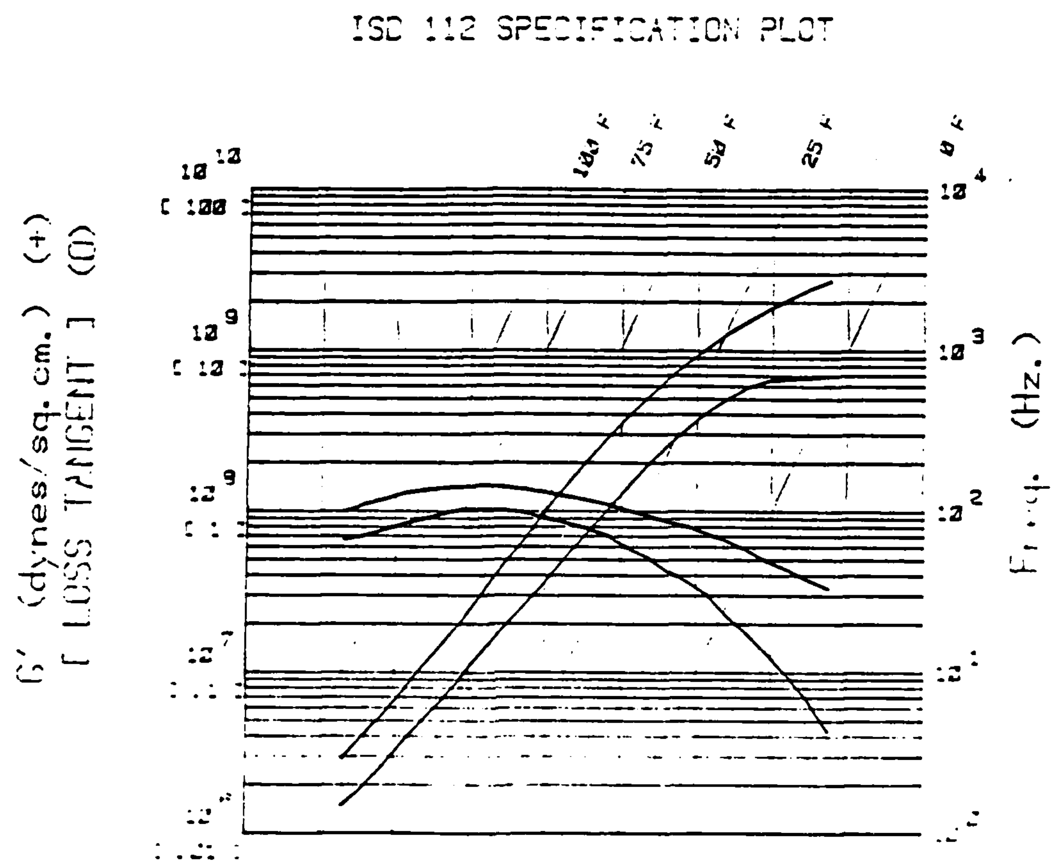

Figure 4.4 3M ISD-112 specification plot.

V. RESULTS

A. MODAL ANALYSIS

A modal analysis was conducted to determine the resonance frequencies and mode shapes for the structure up to 125 Hz. These mode shapes were examined in hopes of determining the best candidates to observe increased damping associated with the microslip phenomenon. This modal analysis and preliminary experimentation was conducted utilizing an impact-decay response and the HP 5451C system previously described in chapter IV. The modal analysis application package operates on measured transfer function data to determine modal properties for the structure. A grid structure was imposed over the model and impact-response data was collected at each grid point. All of this data was then used to determine structural movements associated with each particular mode shape, which occurred at it's characteristic resonance frequency.

From this analysis the first eight mode shapes were determined. Figure 5.1 and 5.2 shows the undeformed shape and grid structure that was utilized for the modal testing. The inner ring was not modeled for the analysis due to the limitation of storage capacity, which determined the maximum number of node points. Figure 5.3 through 5.11 shows the eight mode shapes obtained by the modal analysis. These mode shapes as well as the resonance frequencies agreed closely to a MSC/NASTRAN finite element analysis previously conducted and reported in Reference 19.

The initial objective of the modal analysis was to determine the optimum frequencies to conduct this study

on frictional damping. The optimum frequencies would provide the most differential displacement associated at the contacting surfaces of the joints. These differential displacements would then be used to obtain the frictional damping desired to reduce the structural response. The modal analysis, however, did not provide a clear indication of these optimum frequencies / mode shapes. Due to this uncertainly, a broader low frequency analysis from 15 to 300 Hz was chosen for the remaining analyses.

B. VERIFICATION

Preliminary experimentation was concentrated on ensuring that repeatability could be achieved, both from several input types as well as reestablishment of applied contact force, and minimizing any environmental effects on the model's response. These environmental effects included model orientation, added mass due to a vibration generator versus impact, and boundary conditions imposed by suspension by shock chord.

The vibration generator apparatus which was previously described in chapter IV was next used to conduct a frequency response analysis to compare with the impact-response. The vibration generator process yielded the same resonance frequencies with very slight differences in frequency response amplitudes. These differences were determined to be a function of the filtering utilized by each of the analyzers. When the HP 3562A was replaced by the HP 5451C in Figure 4.3, the frequency response obtained was exact, to that obtained in the impact testing. The added mass associated with the vibration generator was concluded to have no effect on the resonance frequencies or amplitudes. This conclusion is believable due to the fact that the vibration generator and water-proof case

were less than 0.8 percent of the total weight of the model. The orientation of the vibration generator in the gravitational field was also determined to have no effect on the structure's response as confirmed by further orientation experimentation.

Next the boundary condition associated with the shock cord were studied to determine if they had any effect on the structure's response. This investigation changed the attachment location of the shock cord support as well as the length of the shock cord used. Figure 5.12 indicates that the support structure provides no extraneous signals to the model on the orientations tested. This procedure was tested both for impact-response and vibration generator input devices.

The repeatability study was then conducted, in which the entire structure was disassembled and then reassembled again to the same contact force (same bolt torque). The results of this can be seen in Figures 5.13 and 5.14 which indicate that the frequency responses for the grid point located on the vane in the six o'clock position are repeatable. Several grid points were used to confirm the results for the entire structure.

During the repeatability study an interesting phenomenon was observed. A random noise driving input force was utilized because of its fast data sampling rate. However, upon comparison with the slower sampling rate, swept sine driving force, the random noise did not achieve the same resolution. Therefore, the swept sine driving input force was utilized for the rest of the investigation.

During the previously described testing, ten grid points were used to examine the symmetry of the model with respect to the frequency response of the total

structure. The ten grid points were located both on the outer ring as well as the vanes. These locations were chosen to observe the damping effects on the outer structural joints since these joints appeared to have more relative motion across the joint interfaces at lower resonance frequencies. During all of the above experiments, symmetric points produced similar frequency response graphs. These plots were not exact but the structure with the vibration generator installed was not exactly symmetric.

Each swept sine data run was kept to a maximum span of 100 Hz to increase the frequency resolution to 0.5 Hz. Even at this resolution there were several data runs that yielded poor resolution and exact damping calculations could not be obtained. Due to the time required to obtain each data run, only two grid point were utilized for the continuation of this study. The first point was on the outer shell at a 15 degree rotation from the vane with the vibration generator on it and six inches from the front of the model. The other grid point was located on the vane in which the vibration generator was attached, six inches from the back on the model and four inches in from the outer shell. The same results were obtained on either side of the vane joint and only the data obtained from the grid point located on the vane are shown in the figures to follow. All values of the coherence obtained throughout the experimentation were 0.9 or better except in the frequency range of 15 to 23 Hz. This low frequency range is at the lower range of the F4/F7 frequency generator making the reliability of the data hard to confirm.

The applicability of the data obtained in this study was of concern so a vane to system coupling experiment was conducted. This experiment started with

the outer cylinder removed and the four vanes installed at a uniform contact force at each joint. One vane was then removed at a time and the frequency response obtained and compared to that of the four vane response to determine the effects of the deletion of a vane. This type of analysis could be used to determine the effects of the addition of a vane(s) to the structure, as in the case of a turbine compressor system. The results are presented in Figures 5.15 and 5.16. It can be seen that the coupling associated by one vane is very minimal. This is observed by the fact that only slight changes in the frequency response occurred when the vanes are removed (see Figures 5.15 and 5.16). The only significant change occurred when three of the vanes were removed (Figure 5.17). This indicates that our test structure could model a structures with four or more vanes without significant change in the overall results.

C. FRICTION JOINT ANALYSIS

The varying contact force analysis was then conducted in which the bolts were torque to the maximum value, tested and then the torque reduced and tested again.

Figures 5.18 through 5.23 show the frequency response of the model over the frequency range 15 to 115 Hz. In all of these graphs the dotted line is the frequency response of the structure at 100 percent contact pressure, and the solid lines are at a different percentage as labeled with each figure. Figure 5.18 indicates that little or no change is obtained from 100 to 75 percent contact force. The anomalies observed are similar to those obtained during the repeatability studies or were correctable by increasing the resolution. However, due to the time

involved obtaining data, increasing the resolution was not deemed necessary for all resolution problems. It can be seen that the resonance peaks near 100 Hz begin to shift down in frequency at approximately 40 percent contact force with still no indications of any shifting at lower frequencies (see Figure 5.19). This frequency shift is the first observable phenomena that can be obtained even before any damping changes take place. At twenty and again at ten percent the resonance peaks continue to shift to the left or down in frequency (see Figures 5.20 and 5.21). The results at ten percent (Figure 5.21) also indicates the beginning of the low frequencies to shift due to decreased contact force. These trends continue through five and 2.5 percent contact force data runs (Figures 5.22 and 5.23). From the data obtained there was a maximum frequency shift of 8 Hz for the resonance frequencies at approximately 100 Hz associated with the 2.5 percent contact force.

Figures 5.24 through 5.29 are the data obtained for the second 100 Hz frequency analysis. It can be seen that even at the 75 percent datum, there is an observable shift in the frequencies at 127 and 137 Hz. These shift continue as the contact force decreases as before. These resonance frequency continue to shift down in frequency and are also associated with a decrease in resonance amplitudes. The maximum frequency shift observed was 12 Hz, again at the 2.5 percent contact force. Note also that the 100 Hz peak repeats the previously observed effects obtained from the 15 to 115 Hz data runs.

The final frequency range analyzed was from 200 to 300 Hz and is shown in Figures 5.30 through 5.35. This data exhibited the same frequency shifts as before. It was also noted that the amount of frequency shift was not the same at each resonance frequency, this leads to

the possibilities of two resonance frequencies overlapping or adding together. This type phenomena is believed to cause the appearance of a new resonance peak at approximately 256 Hz in Figure 5.31, and is clearly seen in Figure 5.33 at 252 Hz.

In Figure 5.35 the contact force is 2.5 percent and new resonances frequencies associated with totally new mode shapes indicate that the structure has gone from the microslip to the macroslip (total slip) situation. An indication of when this transition takes place can be estimated by when the response reaches its minimum amplitude. This point is seen to be between ten and five percent contact force (see Figures 5.33 and 5.34). The amplitudes associated with 100, 123, 132, 210, and 240 Hz all indicate this transition at this particular contact force. Therefore, the maximum damping should be achieved at this approximate contact force.

Figures 5.36 through 5.38 are plots of percent damping factor versus frequency for each of the previously described data runs. The percent damping factor was determined via the half power point method as described in Reference 17. The damping factor is very sensitive to the frequency resolution and with only a 0.5 Hz resolution the error bars would clearly overlap each consecutive data points and quantitative conclusions from these results are not possible, however general trends in the damping can be observed. It can be seen that the damping increases until it achieves a maximum at the ten percent contact force as previously predicted from the frequency response plots. It is also noteworthy, that the damping factor seem to increase across all resonance frequencies as the contact force decreases instead of only at those particular frequencies observed previously. The

greatest increase in damping factor is still associated with the above mentioned resonances frequencies. These particular resonance frequencies are obviously associated with mode shapes which exhibit the deflections relative to each mating surface. Clearly as a particular mode shape shifts in it's resonance frequency, the damping increases until the mode shape enters into the total slip regime.

Once this study was completed the contact force required to bring the apposing joint surfaces together was determined. This was done by slowly torquing the bolts until a one mil. filler gauge did not pass through the joint clearance. This force was then subtracted off the above contacting forces. The vibration generator's weight was seven pounds and with a friction factor of 0.11 this then is equal to the corrected normal contacting force for 8.8 percent. Clearly the ten percent contacting force is a reasonable result for the force at which the model enters the macroslip area.

D. VISCOELASTIC JOINT ANALYSIS

The 3M ISD-112 viscoelastic material was then introduced between the contact surfaces of the mating joints on the outer ring only. The viscoelastic material was adhered to the outer surface of the vane portion of the joint and the inner structure was lowered into the outer ring. The outer ring was then brought into contact with the material from one side of the joint to the other by torquing to 100 percent torque, from one side of the joint to the other. The total percentage of contact was questioned, and examined upon removal. The actual percentage of contact was estimated at 70 percent, which was much better then expected.

A similar investigational procedure was followed as with the bolt torque determination. Results can be seen in Figures 5.39 through 5.50 in which the dotted lines is the frequency response curve obtained from the 100 percent contact force data run and the solid lines are the frequency response lines for the pictured contact force. The effects of decreased joint contact force are observed earlier than with the bolts only structure at the 75 percent bolt torque (compare Figures 5.18 and 5.39). This effect of shifting the resonance frequencies to the left or down in frequency is accelerated as can be seen when comparing Figures 5.40 and 5.41 with 5.20 and 5.21. However, this shifting is reversed at the lower frequencies as can be observed in the five percent plots (compare Figures 5.42 with 5.22).

Similar results can be observed in the second frequency analysis range from 100 to 200 Hz (see Figures 5.43 through 5.46). The same reversal in frequency shift at about five percent is also observed in this series of plots.

In the final 100 Hz analysis the new resonance peak is already observable in Figure 5.47 and continues to increase in size down to the five percent plot. In the contact force study above this peak first became noticeable at the 20 percent torque and grew quickly, but in the viscoelastic study it was observed at the 75 percent contact force and slowly grew.

Again the percent damping factor versus frequency graph were produced with similar results as those observed previously with the exception that the viscoelastic joints appear not to have reached a breakaway torque where the model slips from the microslip regime into the total slip area(see Figures 5.51 and 5.52). It assumed that the viscoelastic

material provides a large coefficient of friction between the mating surfaces and thus decreases the contact forces required to hold the surfaces together. The graphs seem to indicate that the viscoelastic material is reaching a maximum at approximately five percent, as can be seen in Figure 5.52, as the spacing between the lines become smaller with each decreasing contact force.

The viscoelastic joint plots indicated that a different manifestation is taking place at the joint when the viscoelastic material is added. This manifestation appears to start the shift of resonance frequencies (and thus the damping) earlier and at a faster rate in the higher contact forces but decreases the amount of shift in the lower contact forces.

E. COMPARISON OF FRICTION AND VISCOELASTIC JOINTS

To confirm the previous observation the plots of the same contact force but different joint configuration were graphed.

In Figures 5.53 through 5.67 the dotted lines are the frequency response of the joints with no viscoelastic material added and the solid lines are the frequency response of the joints with viscoelastic material added. Each graph is at one particular contact force as labeled.

Figure 5.53 shows the viscoelastic resonance frequency at approximately 100 Hz to the right of the non-viscoelastic peak, however as the contact pressure decreases the viscoelastic peak shifts at a faster rate as can be seen in Figures 5.54 through 5.56. Then as the non-viscoelastic peak slips into the macroslip regime, its peak slips at a faster rate and shows up to the left of the viscoelastic peak at five percent contact force (see Figure 5.57). This observation is

seen again in the second analysis band (100-200 Hz) at 100 Hz, 126 Hz, and 136Hz (see Figures 5.58 trough 5.61), however the peaks at 126 and 136 Hz start to the left and increase their distant from the non-viscoelastic peaks until the ten percent contact force, then from ten to five percent the non-viscoelastic peaks again shift at a faster rate and close back in on the viscoelastic peaks (see Figure 5.62). Also note that the viscoelastic resonance peaks have a decreased amplitude as compared to that of the non-viscoelastic peaks at 126 and 136 Hz.

The final analysis band produced the most interesting phenomenon, the resonance peaks associated with the viscoelastic joints moved in both direction as compared to its counterpart on the non-viscoelastic joints (see Figure 5.63). However the trends mentioned above still held true, both in frequency shifts and amplitudes (see Figures 5.63 through 5.67). Of particular note is the appearance of the third peak at 256 Hz early at 75 percent contact force in the viscoelastic joints, which was mirrored at 20 percent by the non-viscoelastic joint.

The plots of the percent damping factor versus frequency for the viscoelastic and non-viscoelastic joints at a set contact force are shown in Figures 5.68 through 5.71. The damping in the viscoelastic joints, at any resonance frequency, is either equal to or greater than the damping associated with its non-viscoelastic resonance frequency. The smallest gap between the two joints appears to be at the ten percent contact force situation or when the non-viscoelastic joint reaches it maximum damping at just prior to the onset of macroslip.

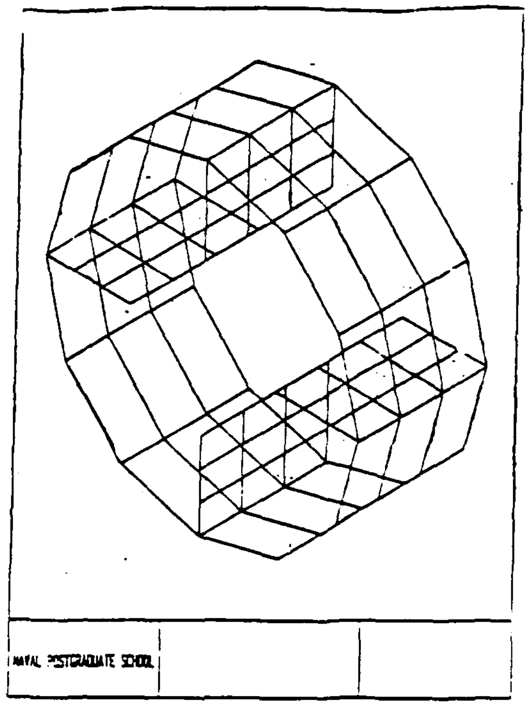

Figure 5.1 Undeformed Shape and Grid Structure.

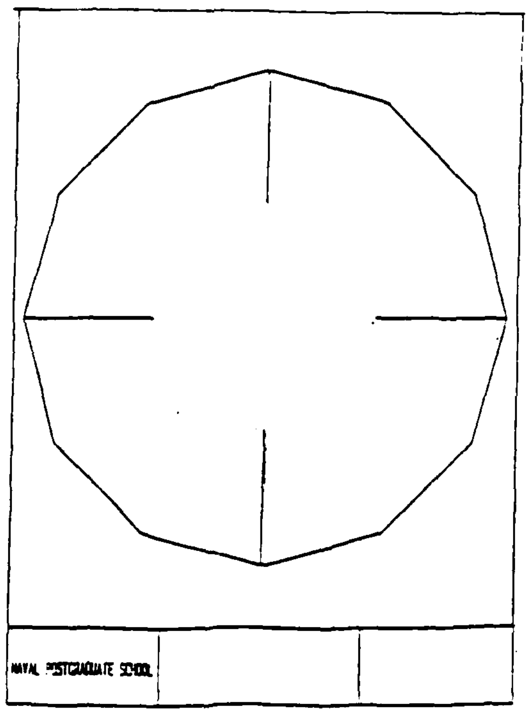

Figure 5.2 Undeformed Shape, Front View.

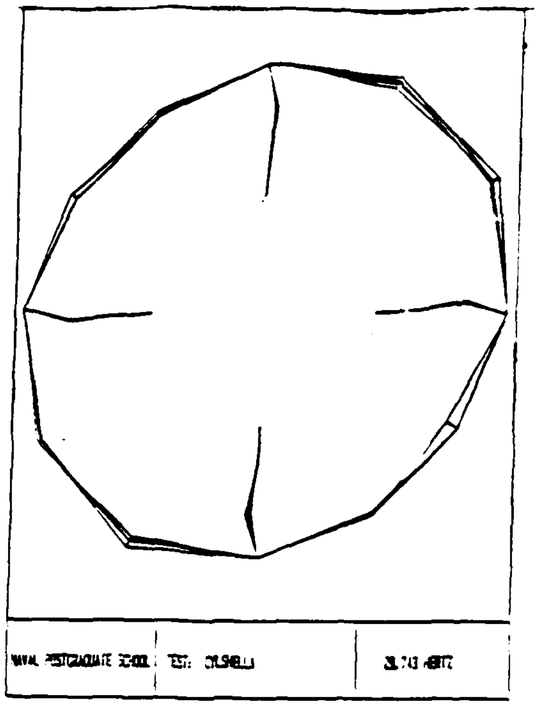

Figure 5.3 The First Free Vibration Mode Shape.

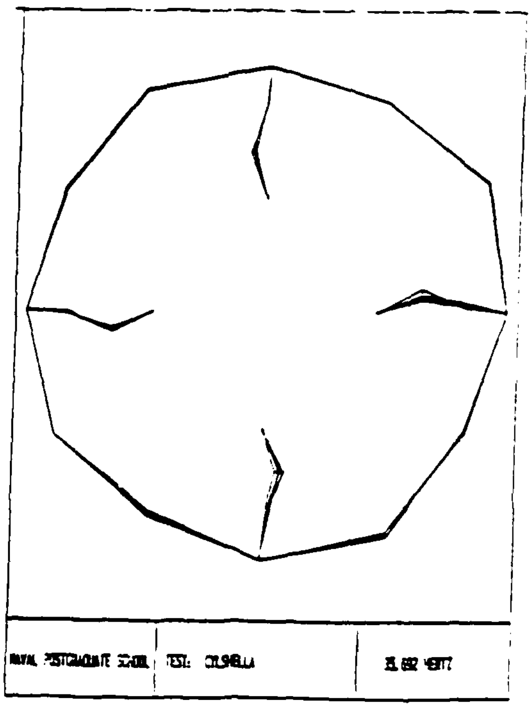

Figure 5.4 The Second Free Vibration Mode Shape.

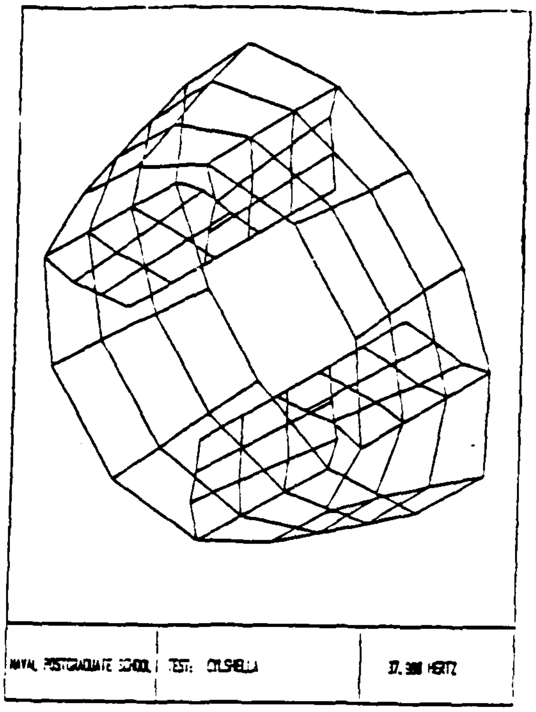

Figure 5.5 The Third Free Vibration Mode Shape (orthographic view)

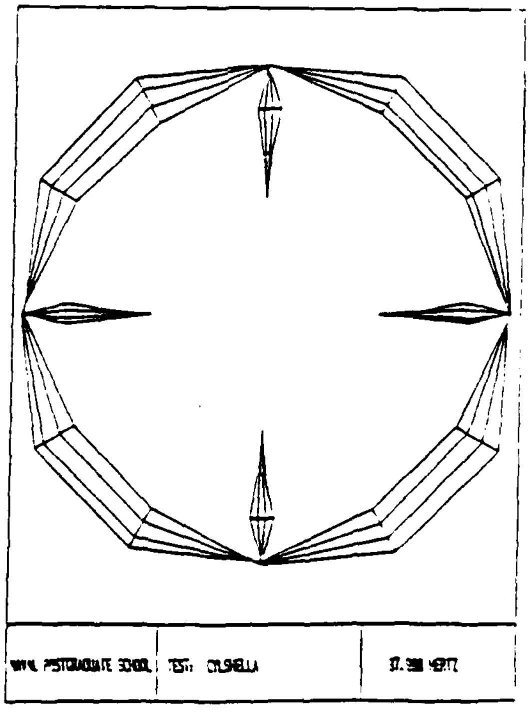

Figure 5.6 The Third Free Vibration Mode Shape (front view)

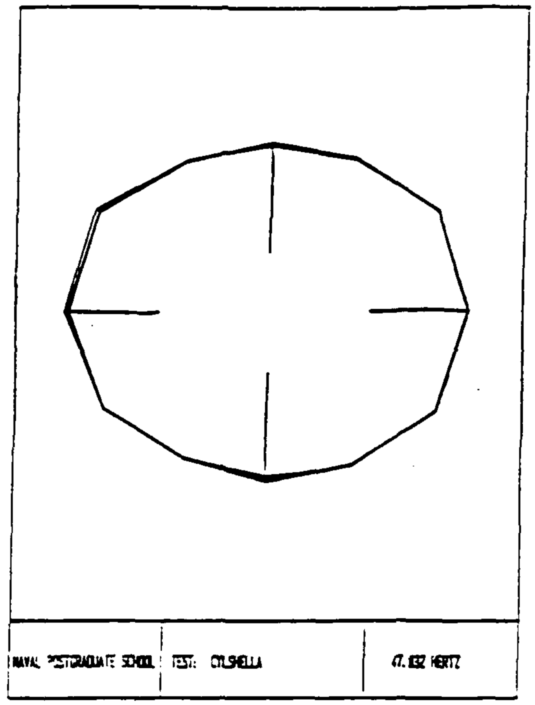

Figure 5.7 The Forth Free Vibration Mode Shape.

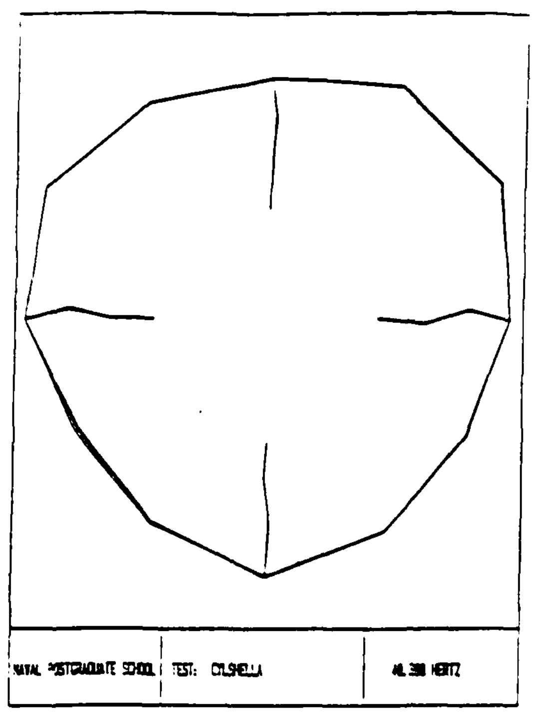

Figure 5.8 The Fifth Free Vibration Mode Shape.

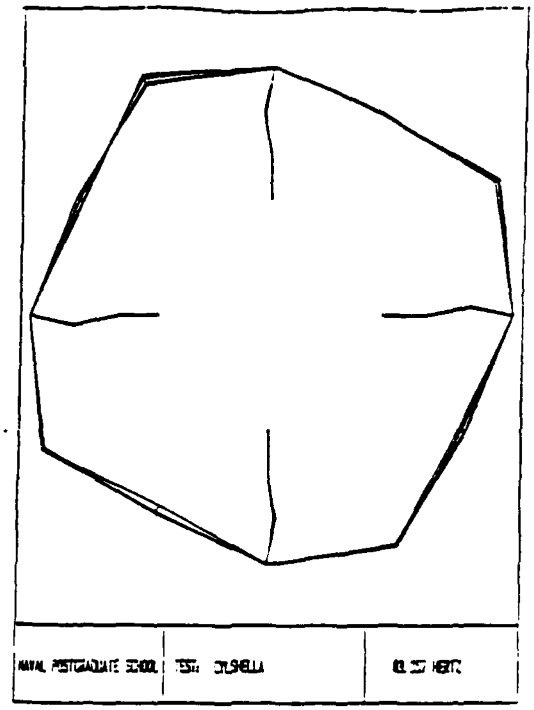

Figure 5.9 The Sixth Free Vibration Mode Shape.

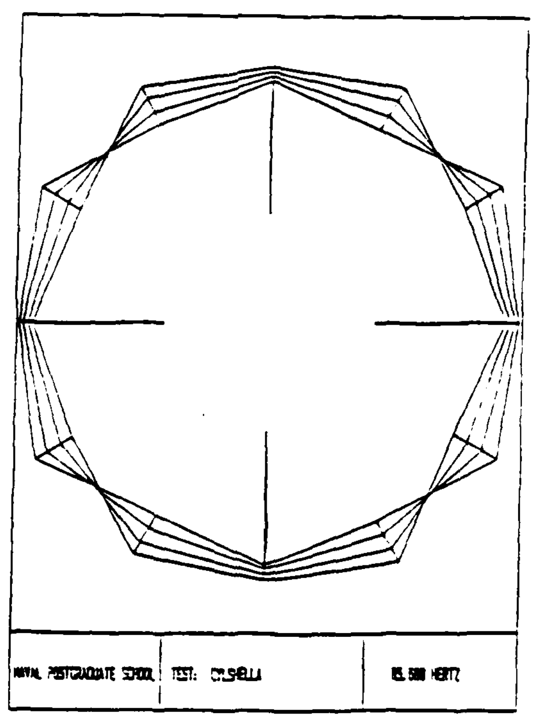

Figure 5.10 The Seventh Free Vibration Mode Shape.

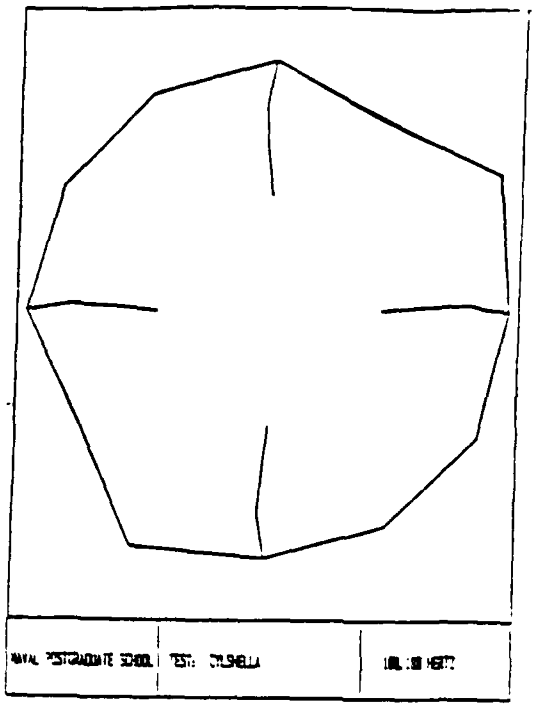

Figure 5.11 The Eighth Free Vibration Mode Shape.

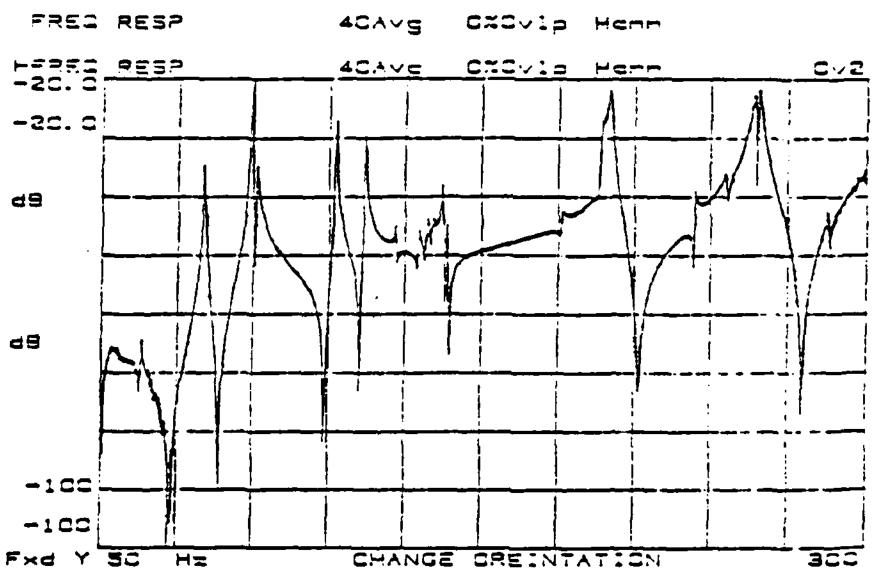

Figure 5.12 Frequency Response Plots of Two Different Free-Free Boundary Conditions and Orientations.

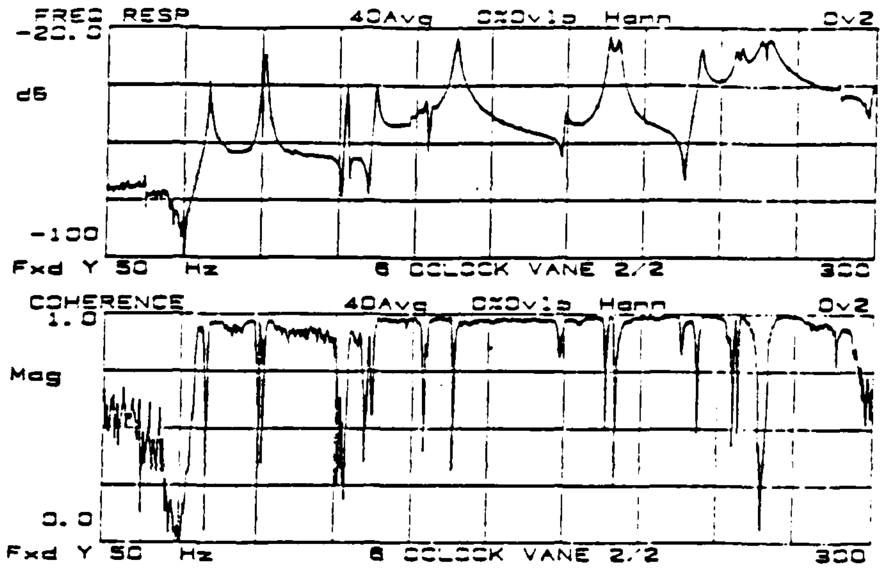

Figure 5.13 Frequency Response of Preliminary 100% Torque.

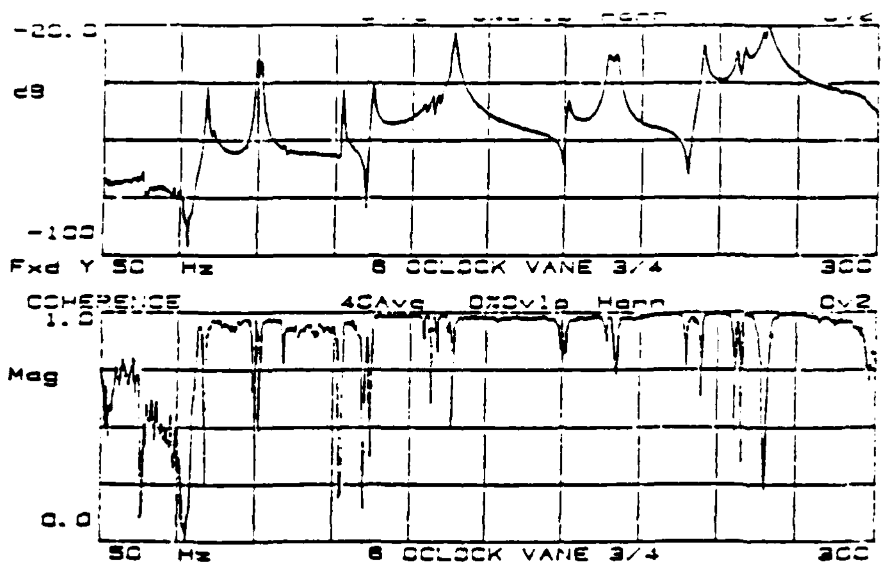

Figure 5.14 Repeatability Frequency Response, Model Disassembled Then Reassemble to 100% Torque.

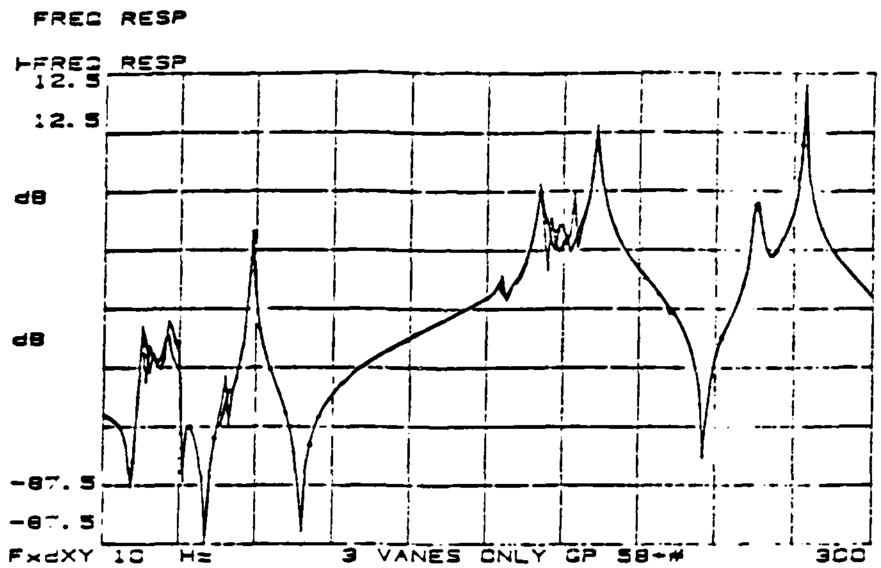

Figure 5.15 Frequency Response of Three Vane Structure Plotted Over Four Vane Frequency Response.

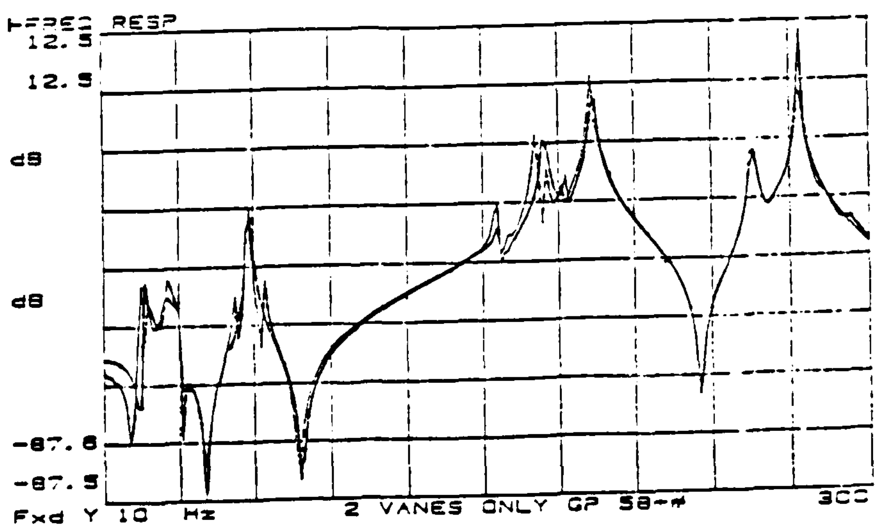

Figure 5.16 Frequency Response of Two Vane Structure Plotted Over Four Vane Frequency Response.

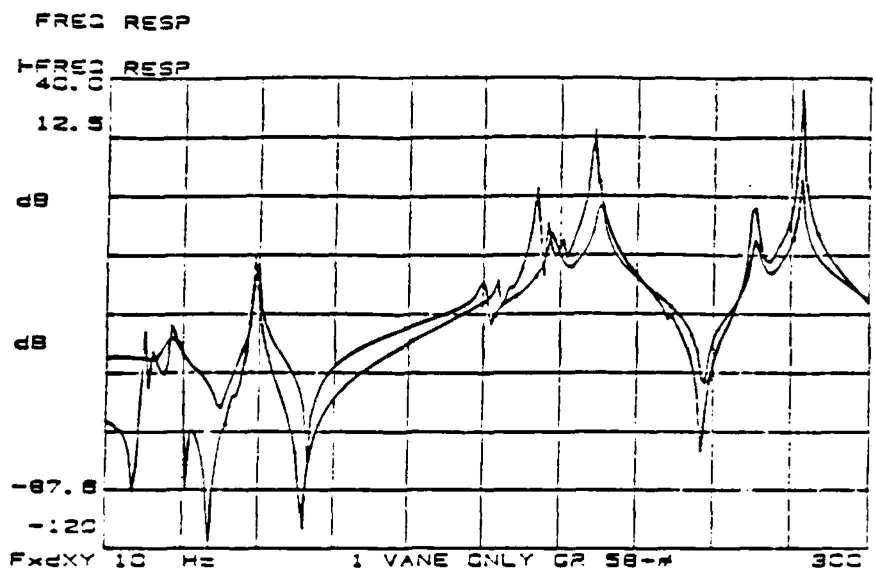

Figure 5.17 Frequency Response of One Vane Structure Plotted Over Four Vane Frequency Response.

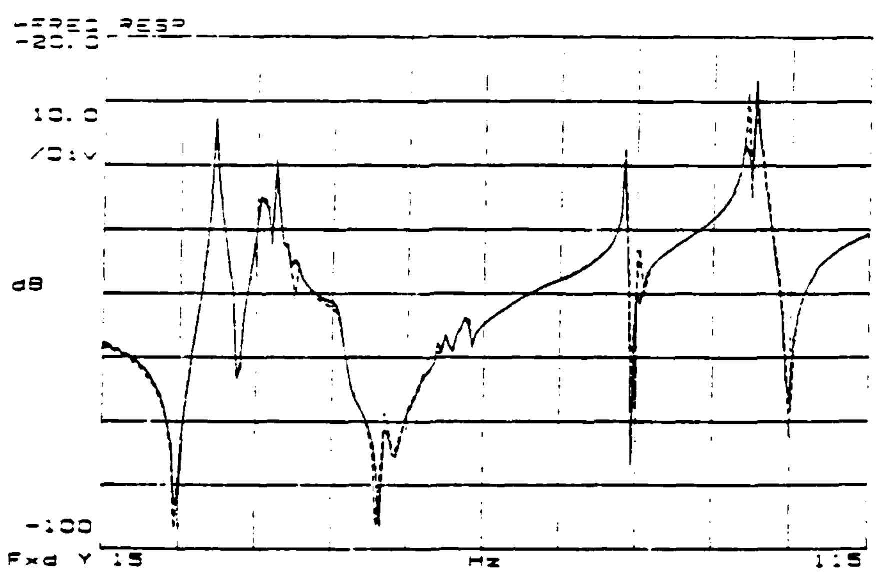

Figure 5.18 Frequency Response of Model at 75% Torque and No Viscoelastic Material. (Dotted Line is 100% Torque)

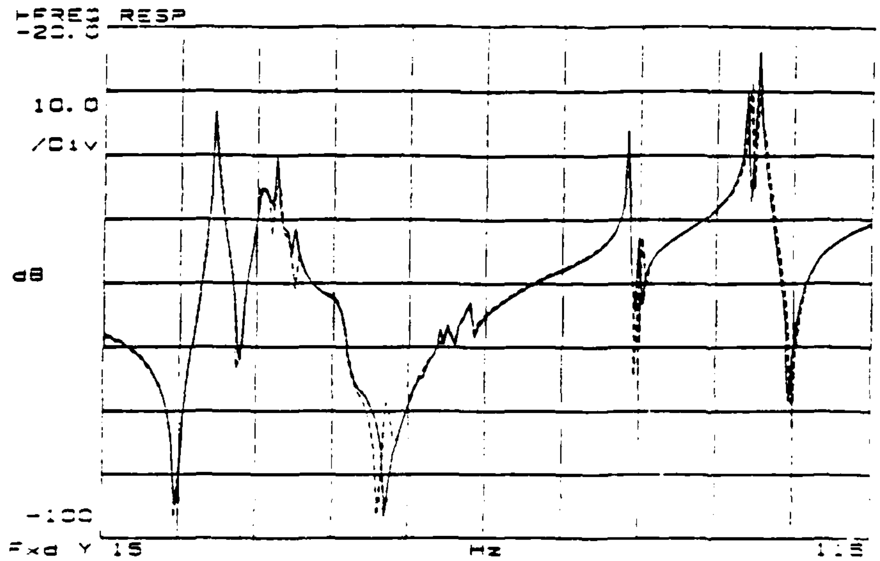

Figure 5.19 Frequency Response of Model at 40% Torque and No Viscoelastic Material. (Dotted line is 100% Torque)

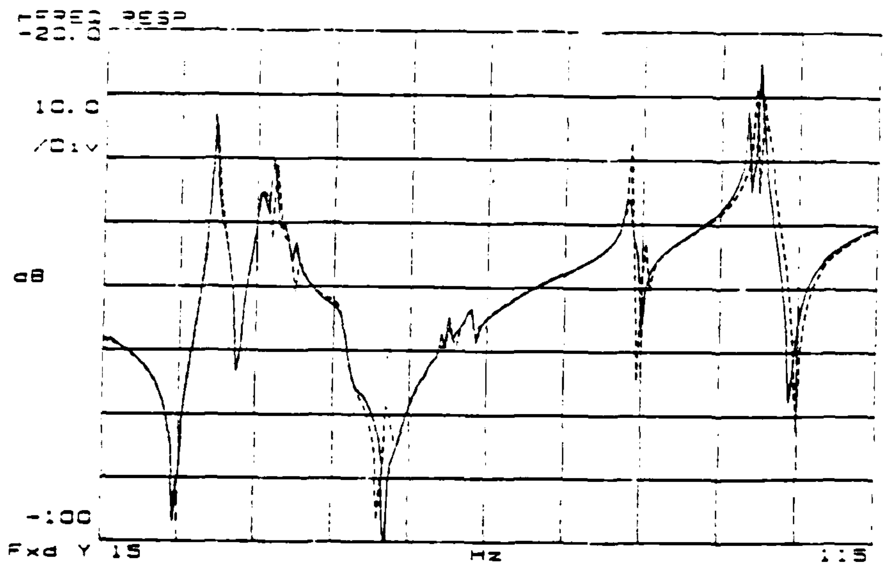

Figure 5.20 Frequency Response of Model at 20% Torque and No Viscoelastic Material. (Dotted line is 100% Torque)

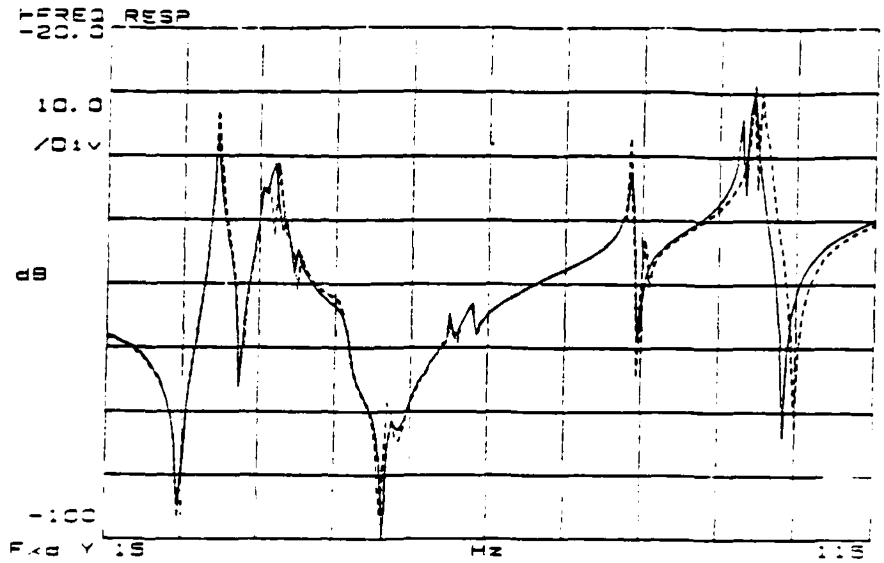

Figure 5.21 Frequency Response of Model at 10% torque and No Viscoelastic Material. (Dotted line is 100% Torque)

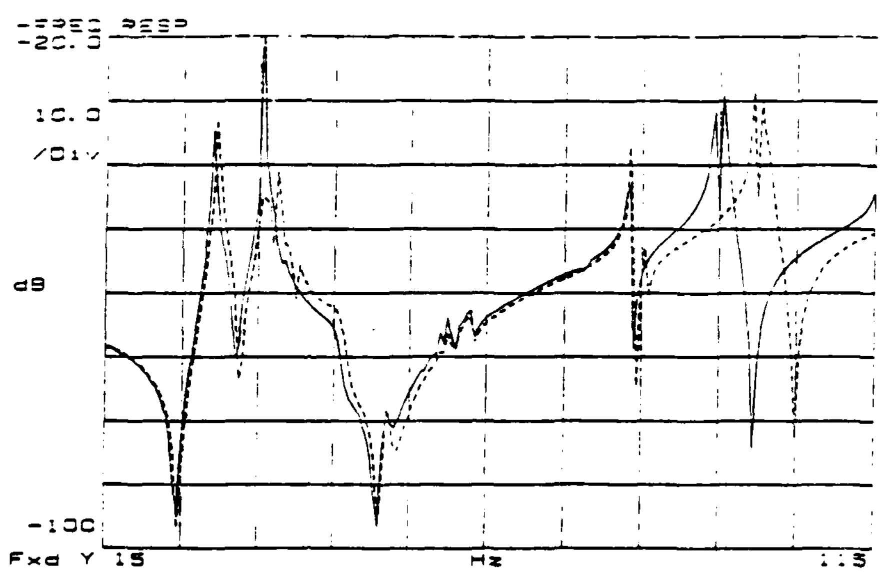

Figure 5.22 Frequency Response of Model at 5% Torque and No Viscoelastic Material. (Dotted line is 100% Torque)

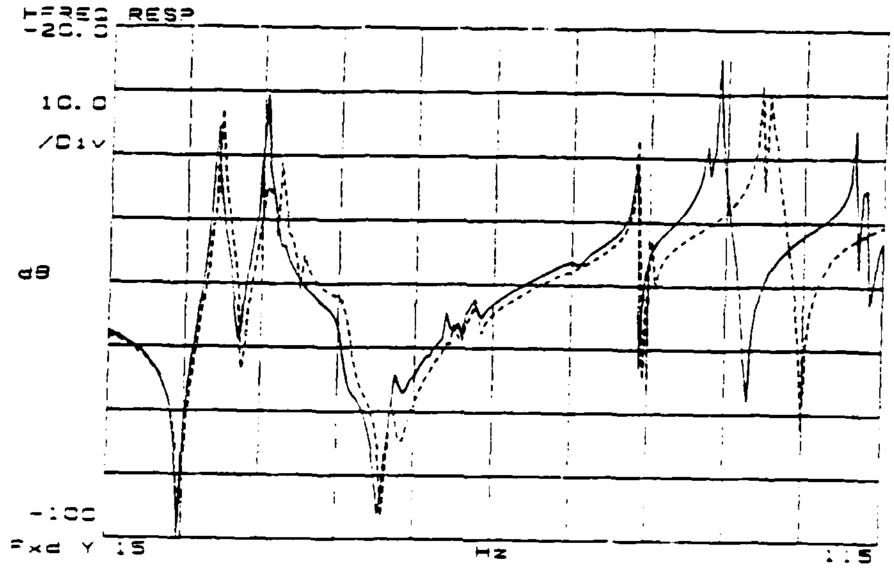

Figure 5.23 Frequency Response of Model at 2.5% Torque and No Viscoelastic Material. (Dotted line is 100% Torque)

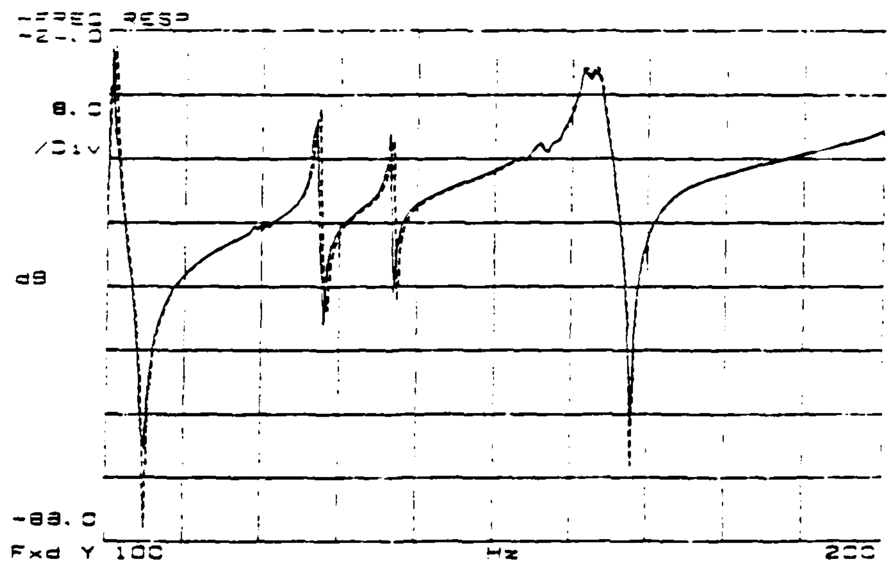

Figure 5.24 Frequency Response of Model at 75% Torque and No Viscoelastic Material. (Dotted line is 100% Torque)

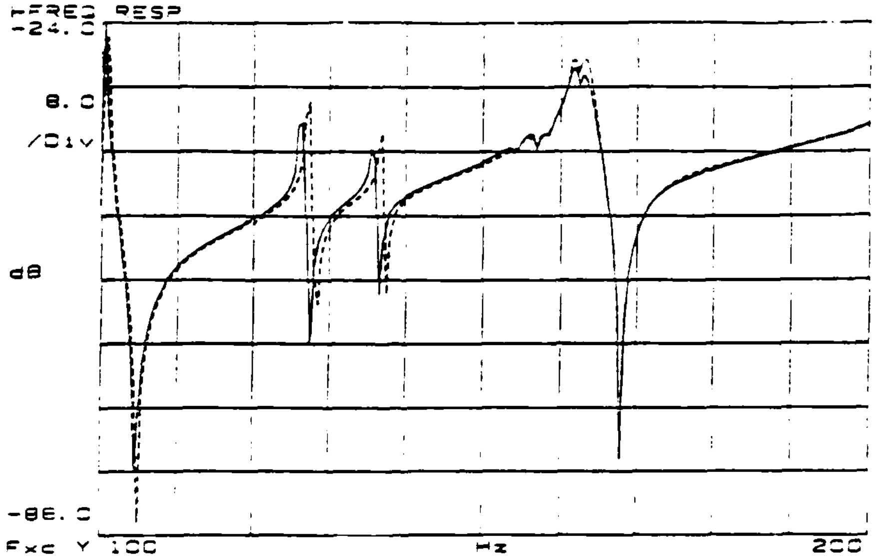

Figure 5.25 Frequency Response of Model at 40% Torque and No Viscoelastic Material. (Dotted line is 100% Torque)

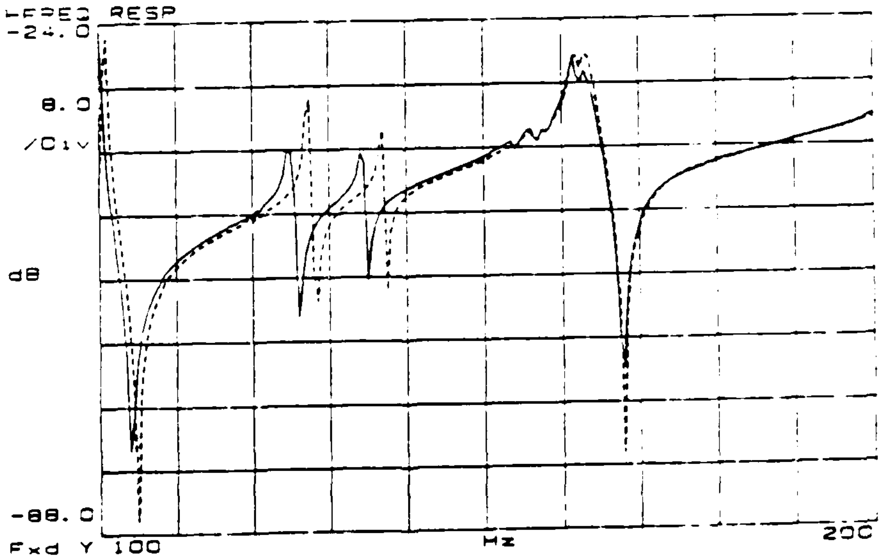

Figure 5.26 Frequency Response of Model at 20% Torque and No Viscoelastic Material. (Dotted line is 100% Torque)

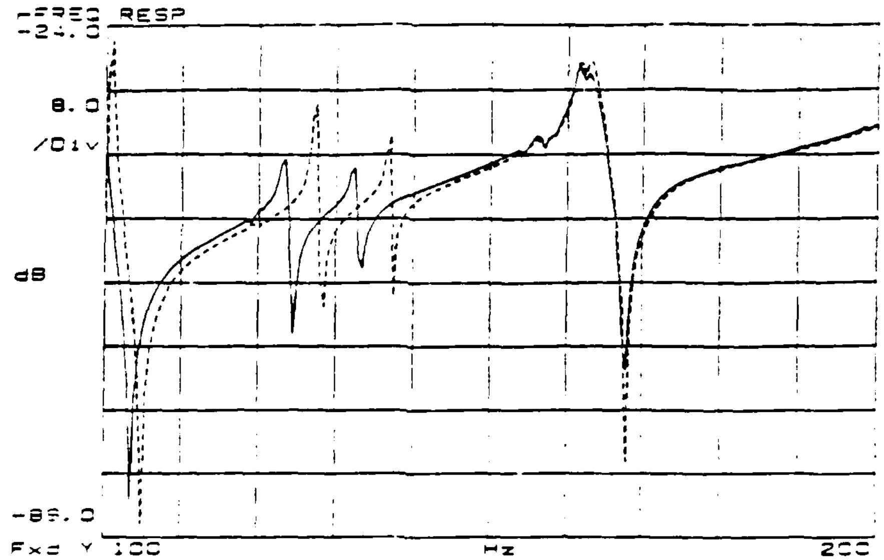

Figure 5.27 Frequency Response of Model at 10% Torque and No Viscoelastic Material. (Dotted Line is 100% Torque)

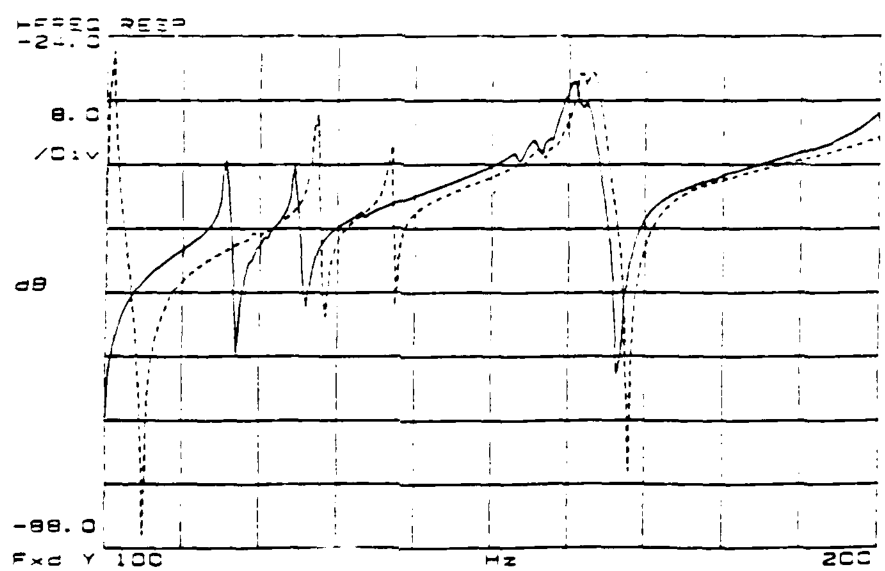

Figure 5.28 Frequency Response of Model at 5% Torque and No Viscoelastic Material. (Dotted Line is 100% Torque)

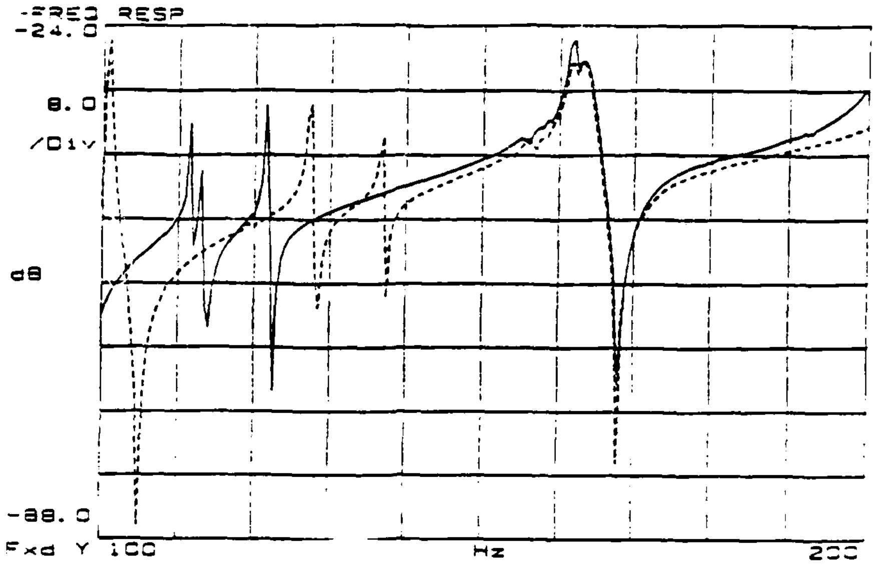

Figure 5.29 Frequency Response of Model at 2.5% Torque and No Viscoelastic Material. (Dotted Line is 100% Torque)

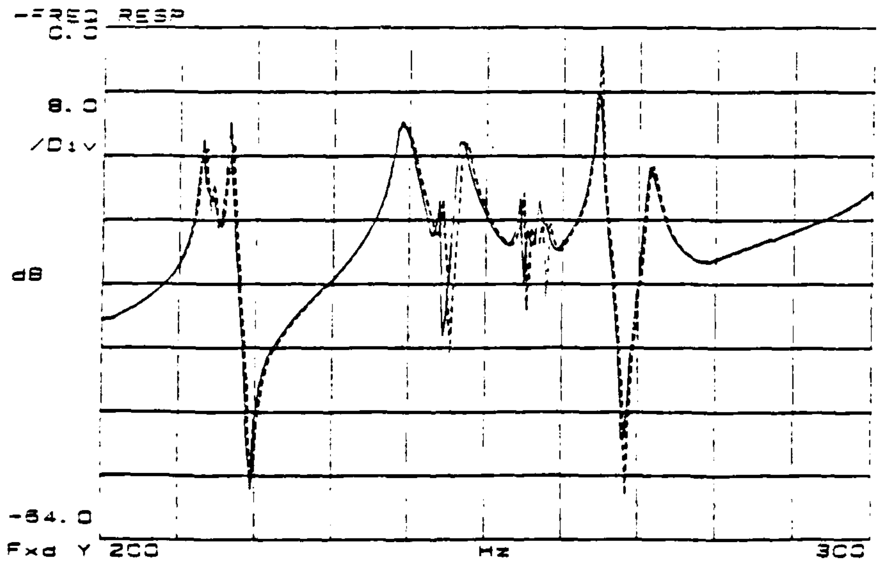

Figure 5.30 Frequency Response of Model at 75% Torque and No Viscoelastic Material. (Dotted Line is 100% Torque)

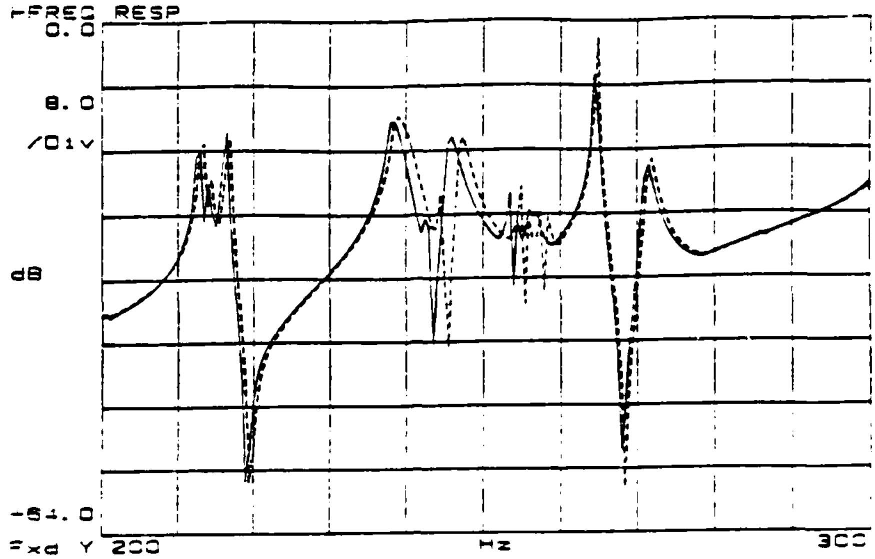

Figure 5.31 Frequency Response of Model at 40% Torque and No Viscoelastic Material. (Dotted Line is 100% Torque)

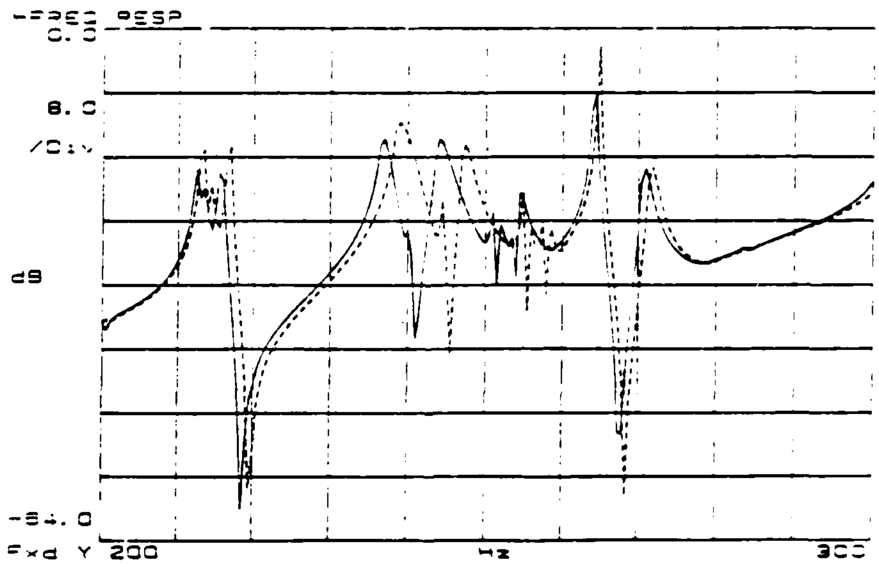

Figure 5.32 Frequency Response of Model at 20% Torque and No Viscoelastic Material. (Dotted Line is 100% Torque)

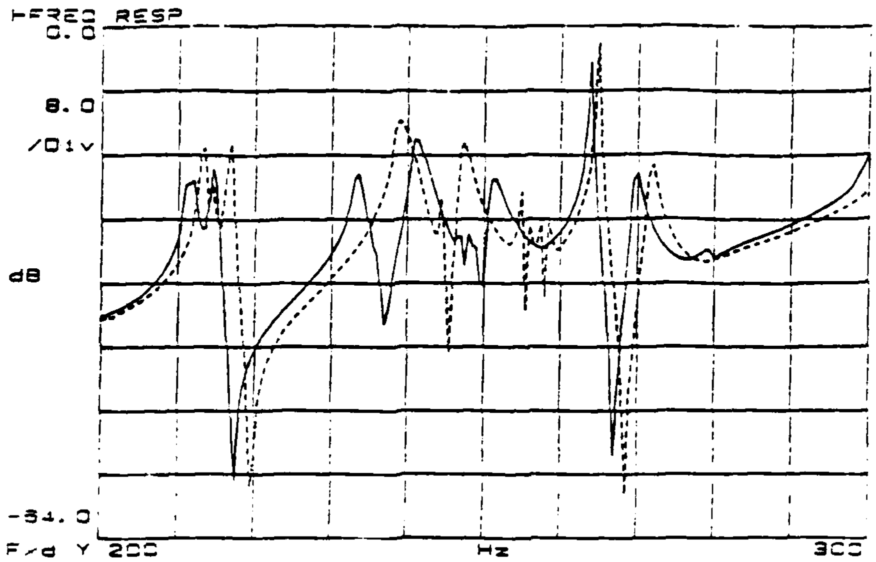

Figure 5.33 Frequency Response of Model at 10% Torque and No Viscoelastic Material. (Dotted Line is 100% Torque)

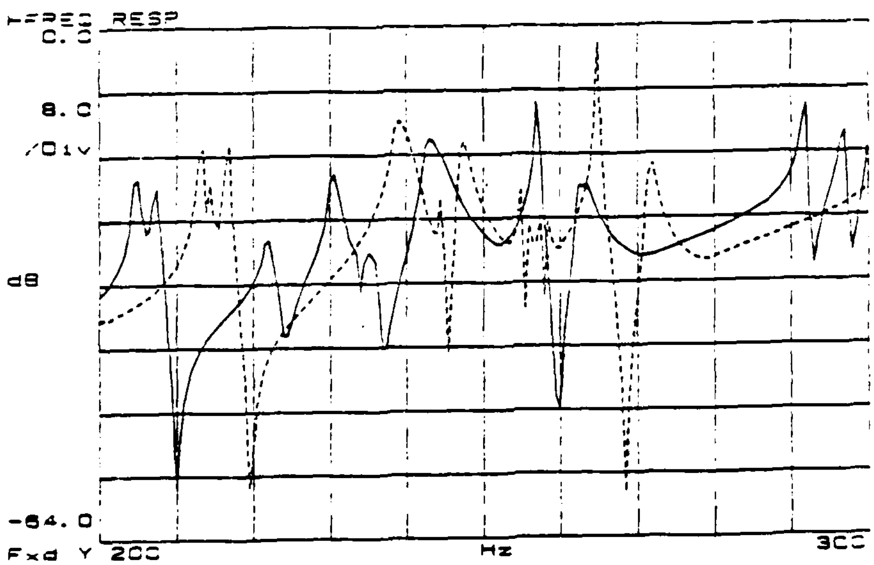

Figure 5.34 Frequency Response of Model at 5% Torque and No Viscoelastic Material. (Dotted Line is 100% Torque)

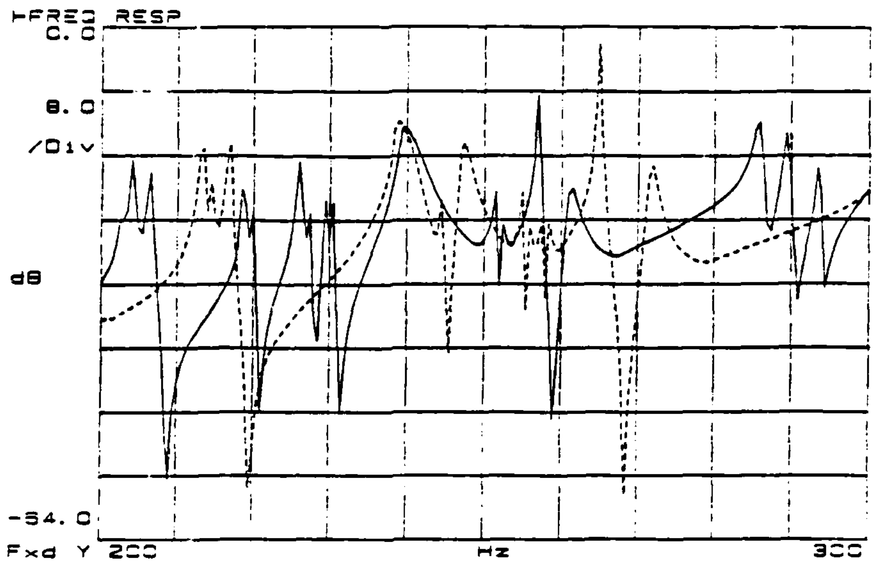

Figure 5.35 Frequency Response of Model at 2.5% Torque and No Viscoelastic Material. (Dotted Line is 100% Torque)

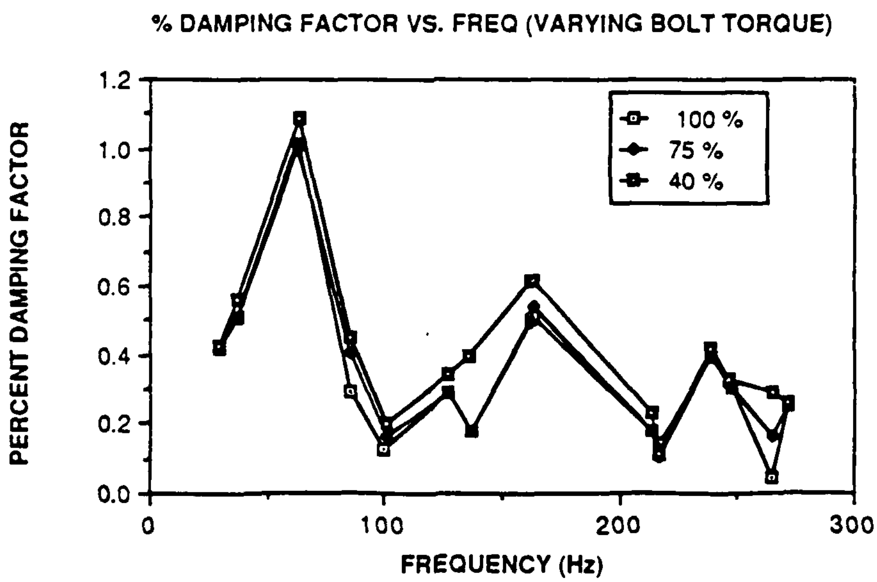

Figure 5.36 Percent Damping Factor for the No Viscoelastic Joint.

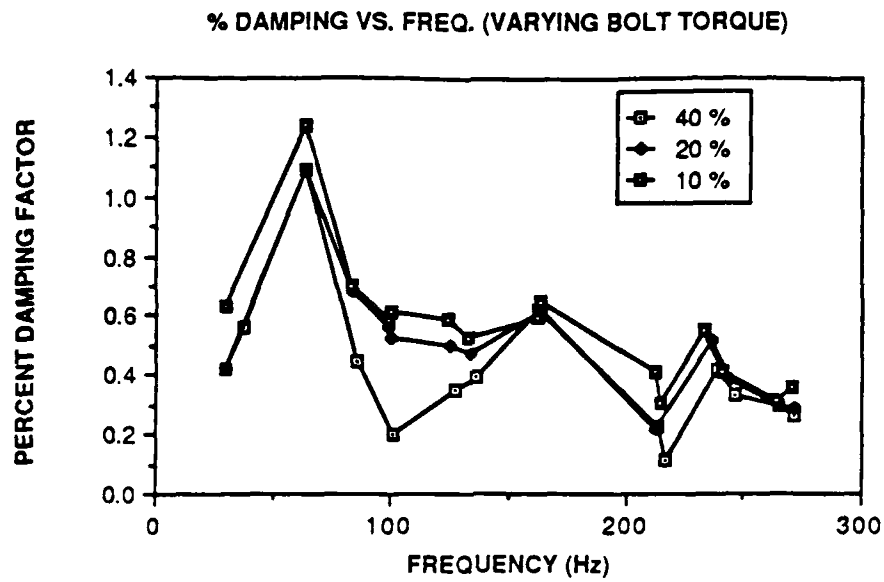

Figure 5.37 Percent Damping Factor for the No Viscoelastic Joint.

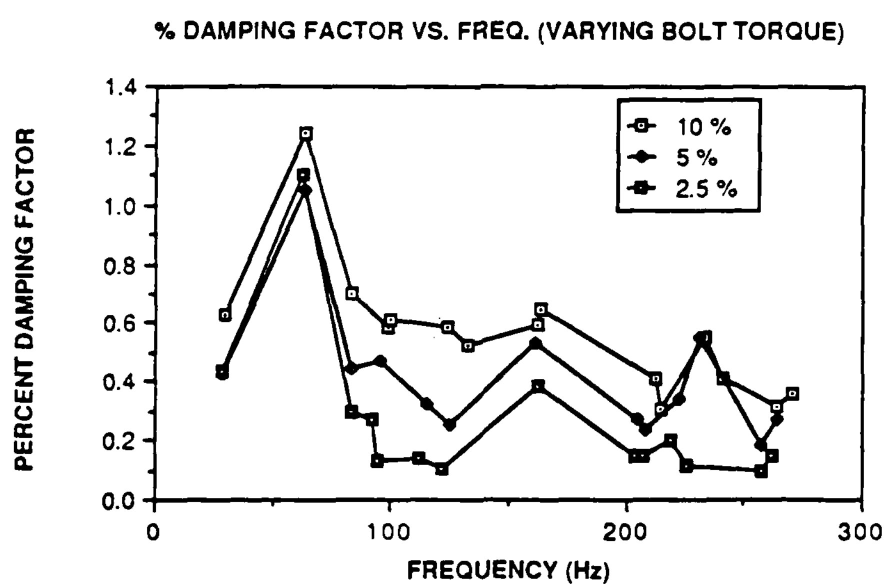

Figure 5.38 Percent Damping Factor for the No Viscoelastic Joint.

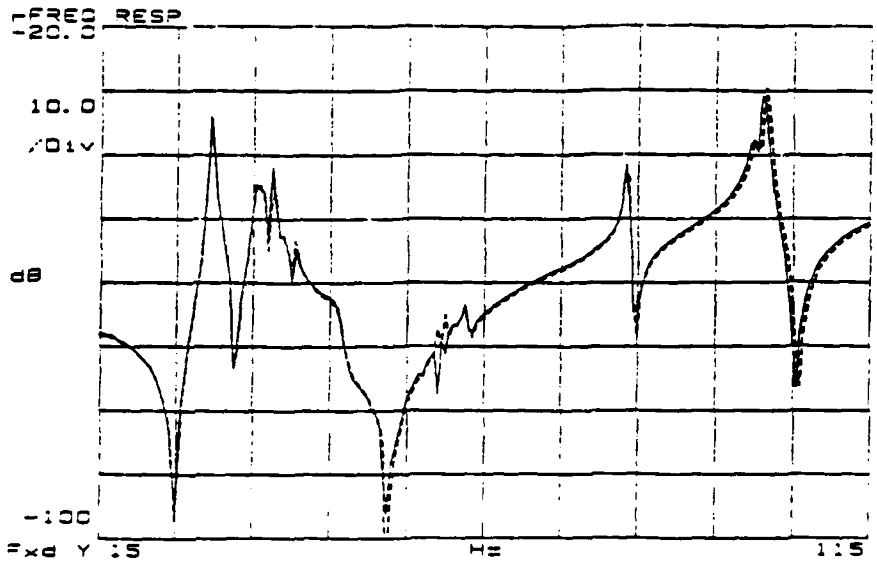

Figure 5.39 Frequency Response of Model at 75% Torque and Viscoelastic Material. (Dotted Line is 100% Torque)

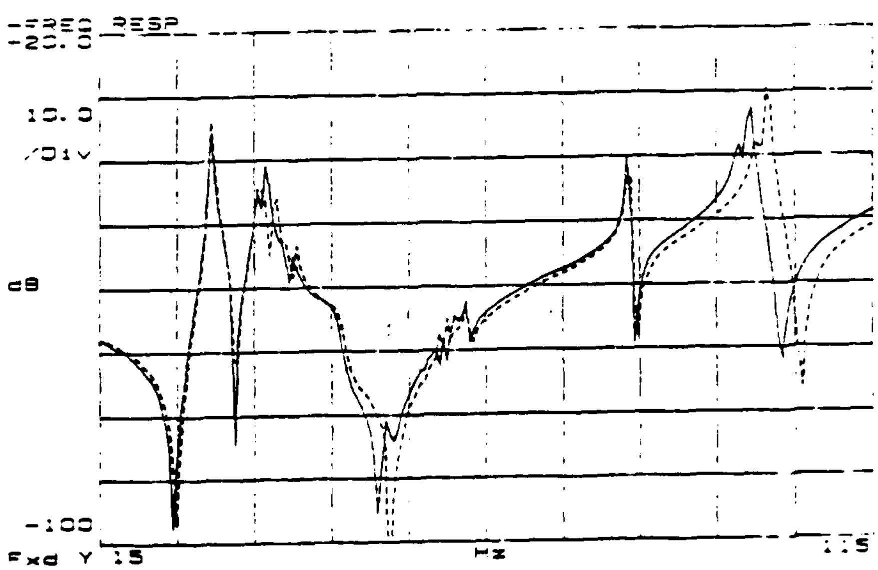

Figure 5.40 Frequency Response of Model at 20% Torque and Viscoelastic Material. (Dotted Line is 100% Torque)

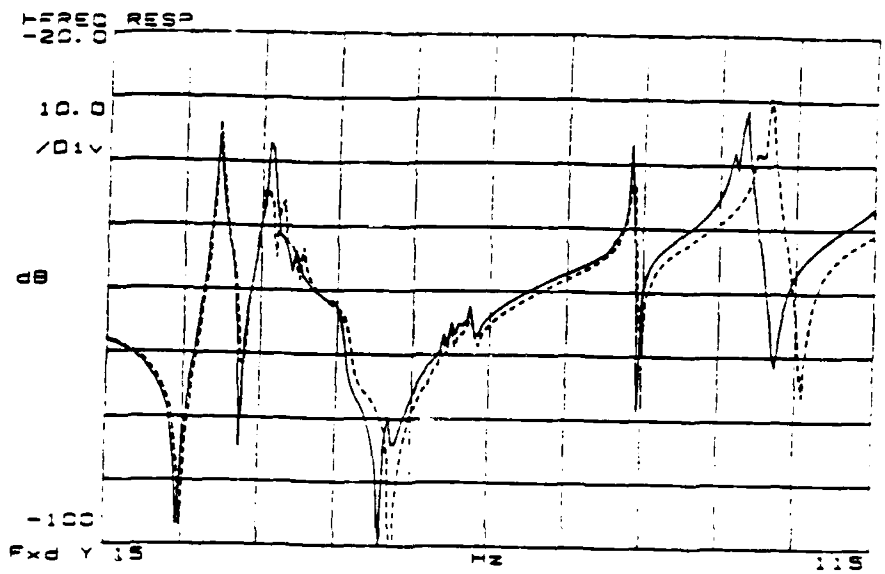

Figure 5.41 Frequency Response of Model at 10% Torque and Viscoelastic Material. (Dotted Line is 100% Torque)

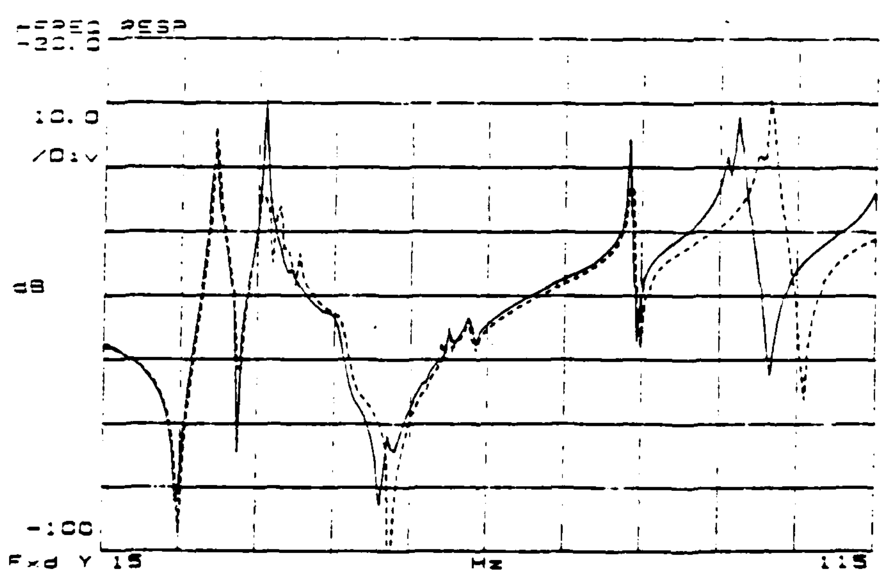

Figure 5.42 Frequency Response of Model at 5% Torque and Viscoelastic Material (Dotted Line is 100% Torque)

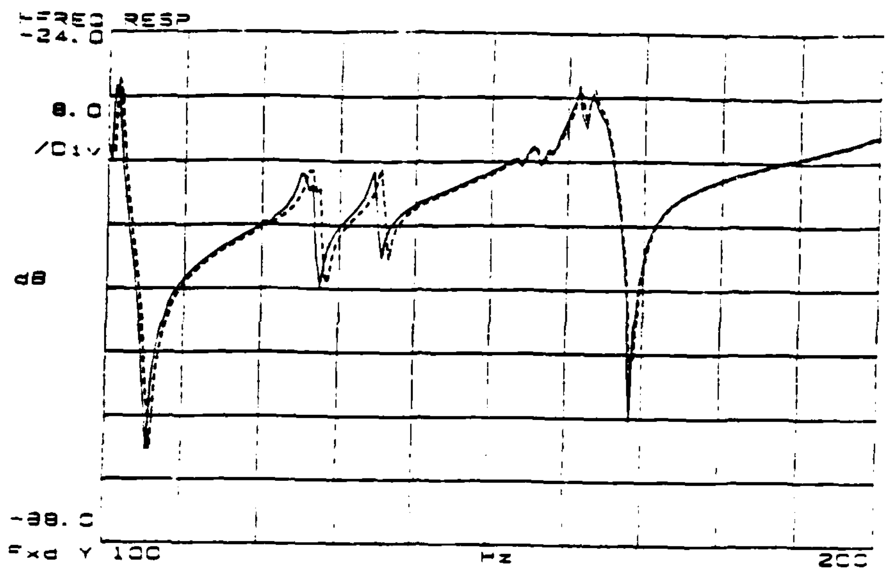

Figure 5.43 Frequency Response of Model at 75% Torque and Viscoelastic Material. (Dotted Line is 100% Torque)

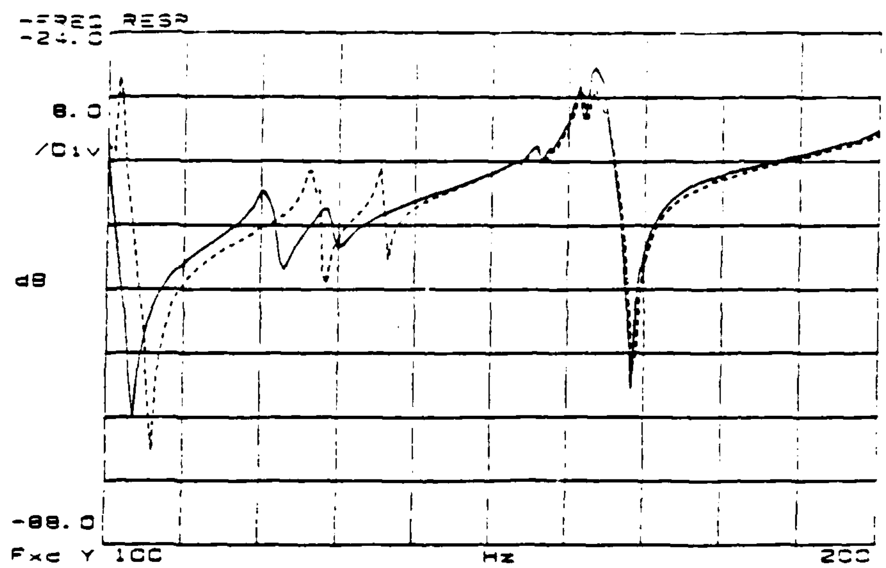

Figure 5.44 Frequency Response of Model at 20% Torque and Viscoelastic Material. (Dotted Line is 100% Torque)

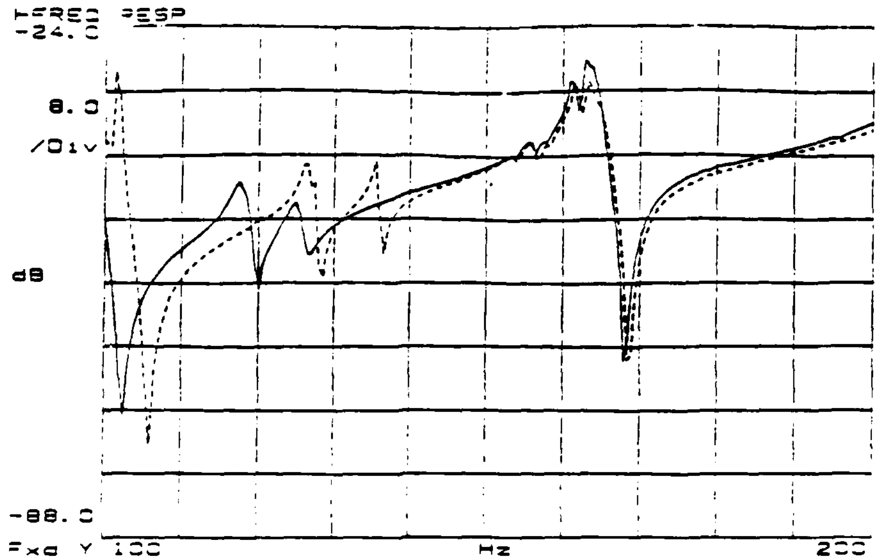

Figure 5.45 Frequency Response of Model at 10% Torque and Viscoelastic Material. (Dotted Line is 100% Torque)

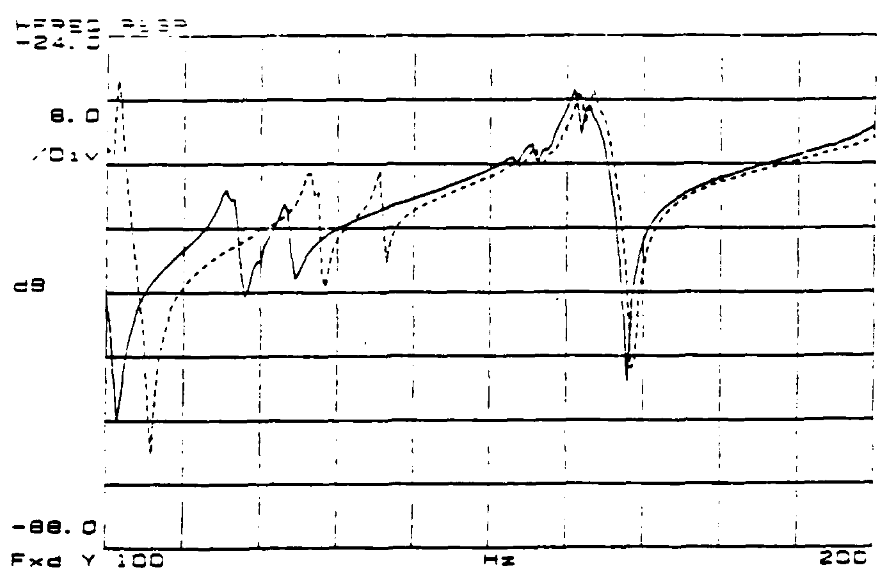

Figure 5.46 Frequency Response of Model at 5% Torque and Viscoelastic Material. (Dotted Line is 100% Torque)

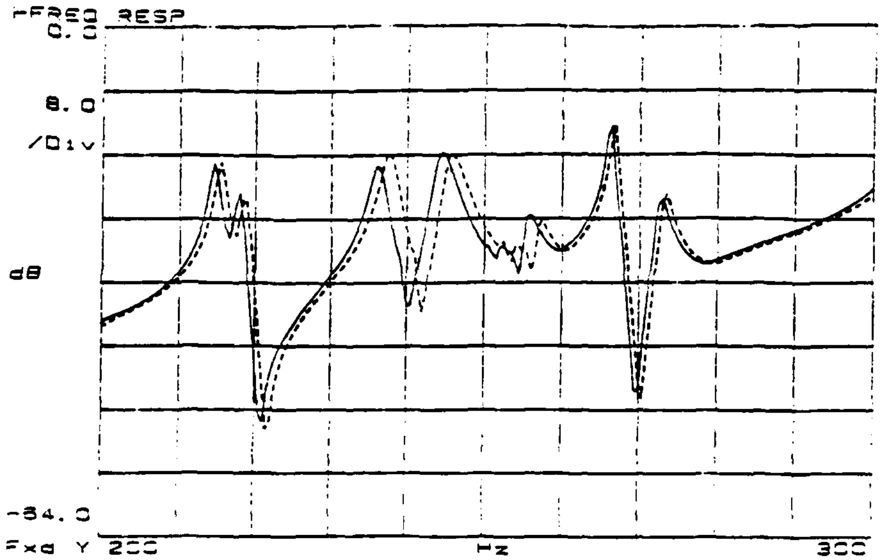

Figure 5.47 Frequency Response of Model at 75% Torque and Viscoelastic Material. (Dotted Line is 100% Torque)

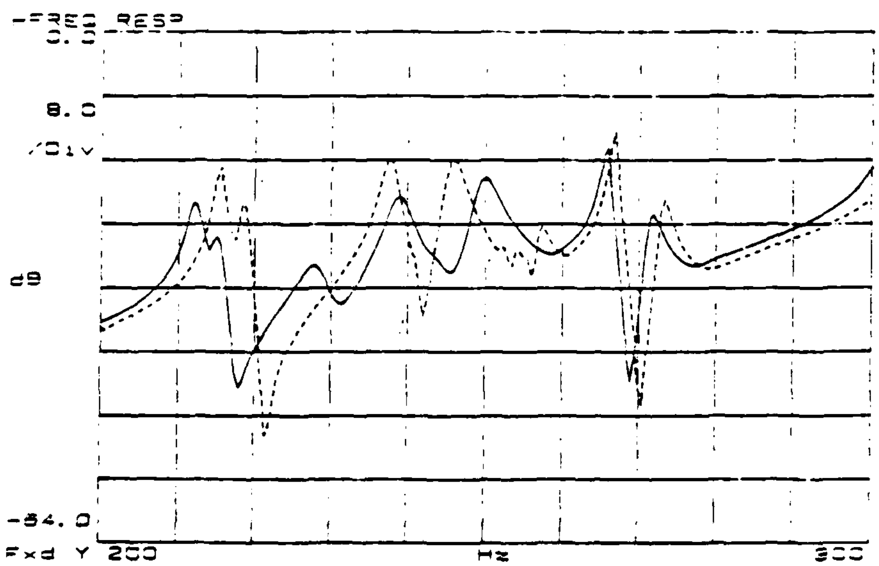

Figure 5.48 Frequency Response of Model at 20% Torque and Viscoelastic Material. (Dotted Line is 100% Torque)

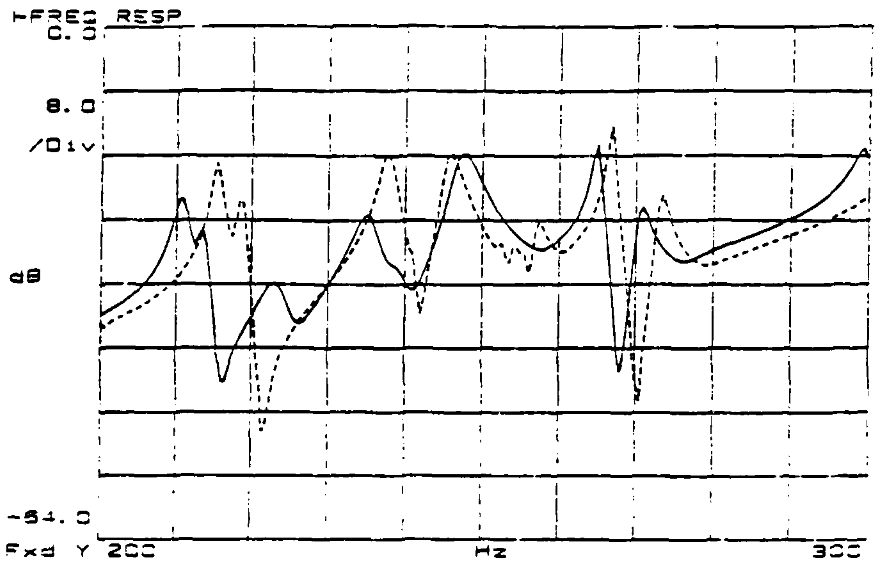

Figure 5.49 Frequency Response of Model at 10% Torque and Viscoelastic Material. (Dotted Line is 100% Torque)

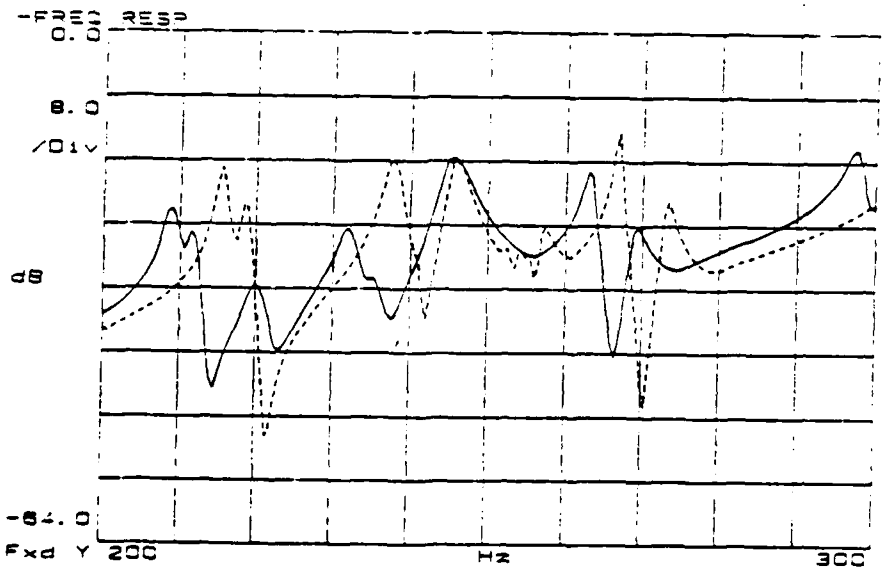

Figure 5.50 Frequency Response of Model at 5% Torque and Viscoelastic Material. (Dotted Line is 100% Torque)

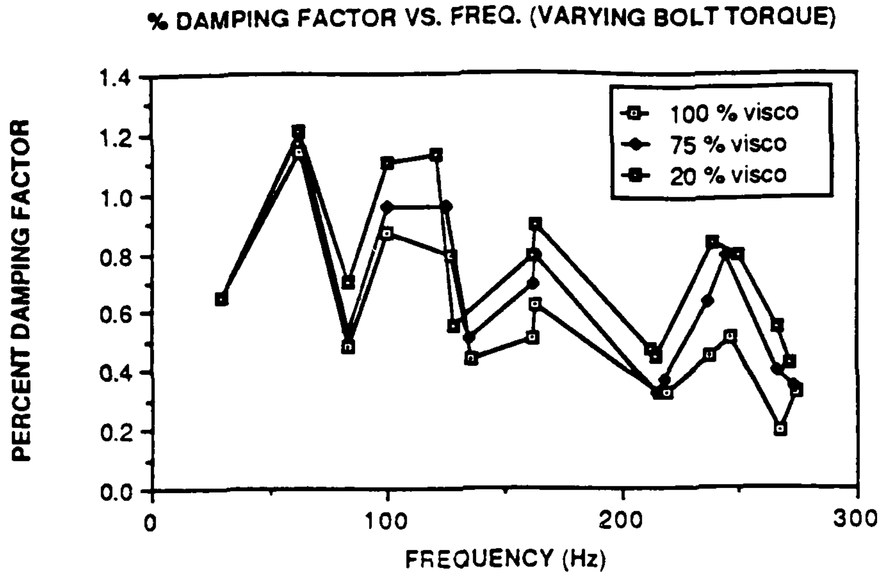

Figure 5.51 Percent Damping Factor for the Viscoelastic Joint.

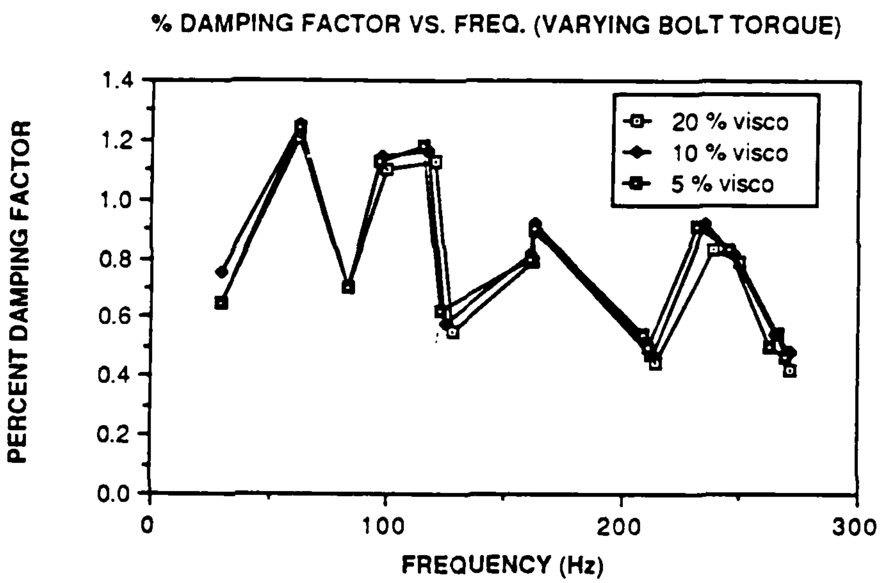

Figure 5.52 Percent Damping Factor for the Viscoelastic Joint.

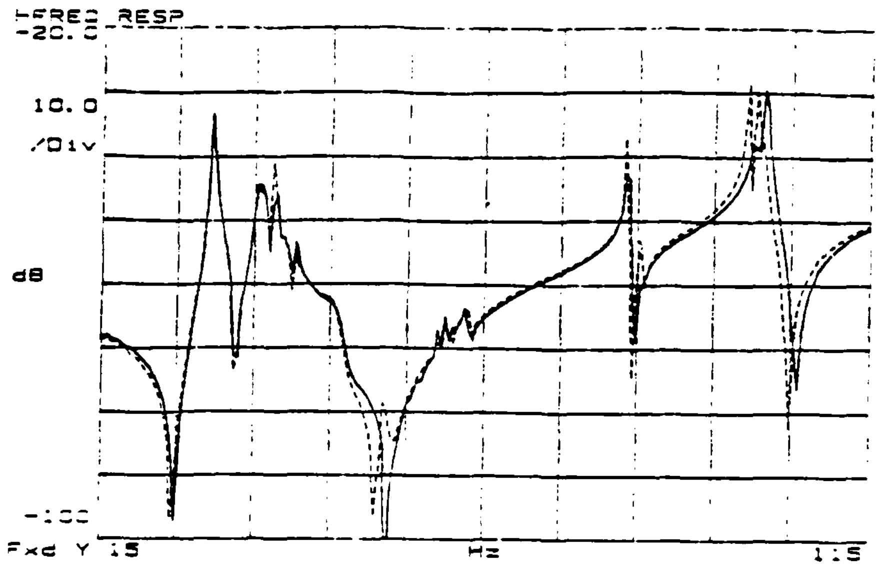

Figure 5.53 Frequency Response of the Viscoelastic Joint at 100% Torque.
(Dotted line is Non-Viscoelastic Joint)

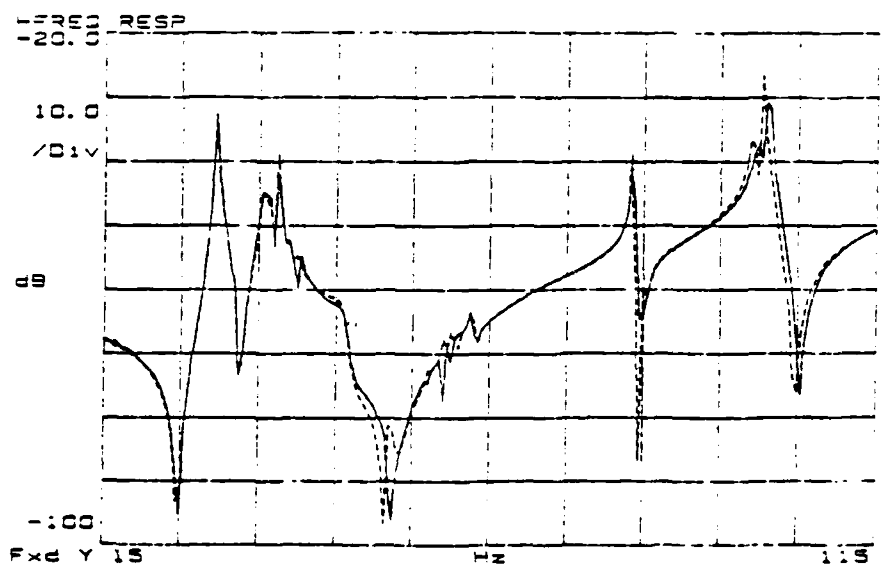

Figure 5.54 Frequency Response of the Viscoelastic Joint at 75% Torque.
(Dotted line is Non-Viscoelastic Joint)

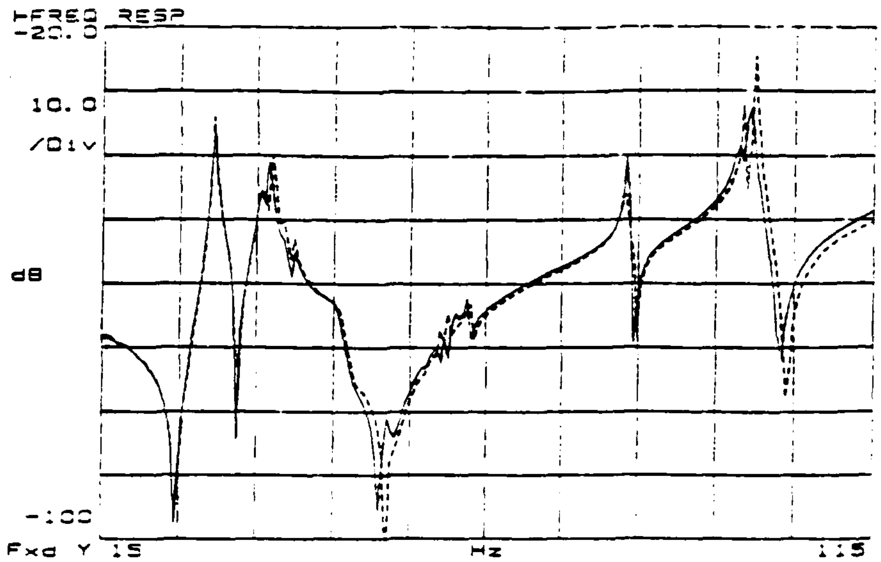

Figure 5.55 Frequency Response of the Viscoelastic Joint at 20% Torque.
(Dotted line is Non-Viscoelastic Joint)

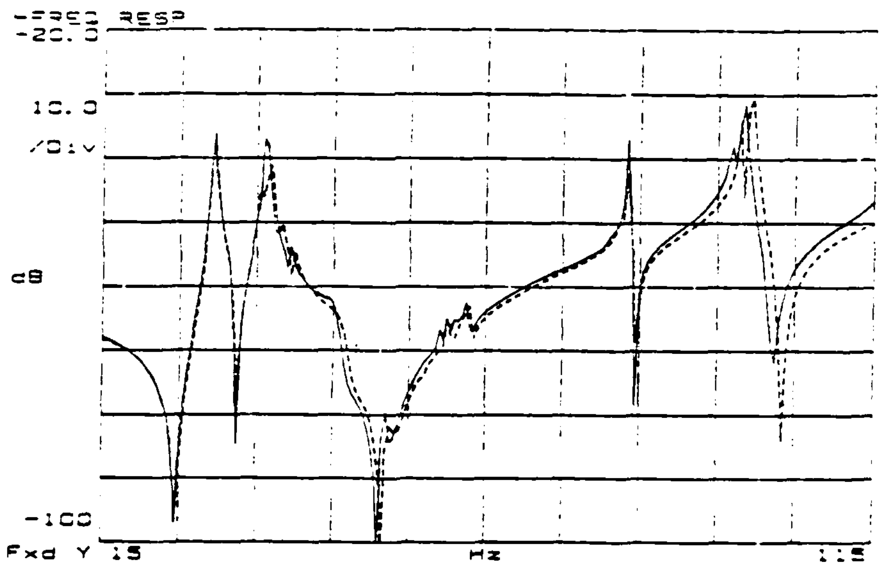

Figure 5.56 Frequency Response of the Viscoelastic Joint at 10% Torque.
(Dotted line is Non-Viscoelastic Joint)

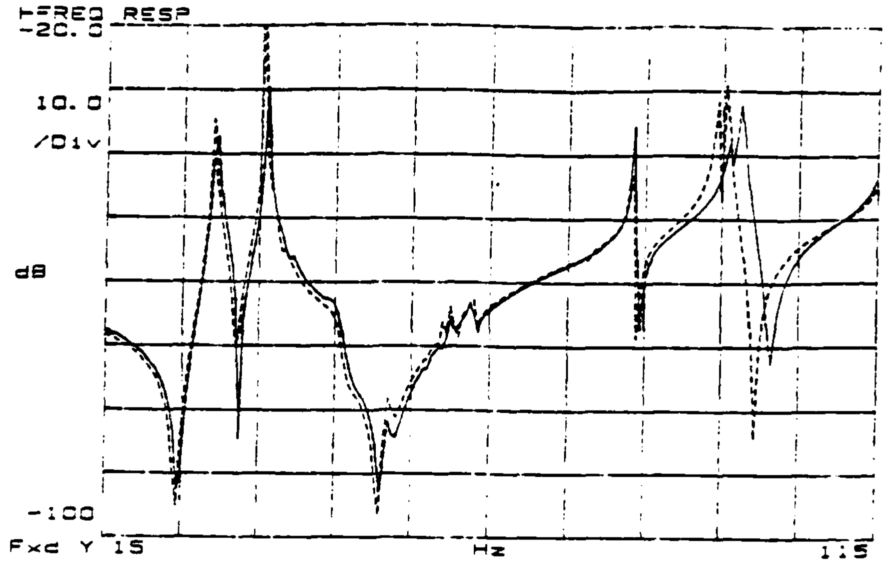

Figure 5.57 Frequency Response of the Viscoelastic Joint at 5% Torque.
(Dotted line is Non-Viscoelastic Joint)

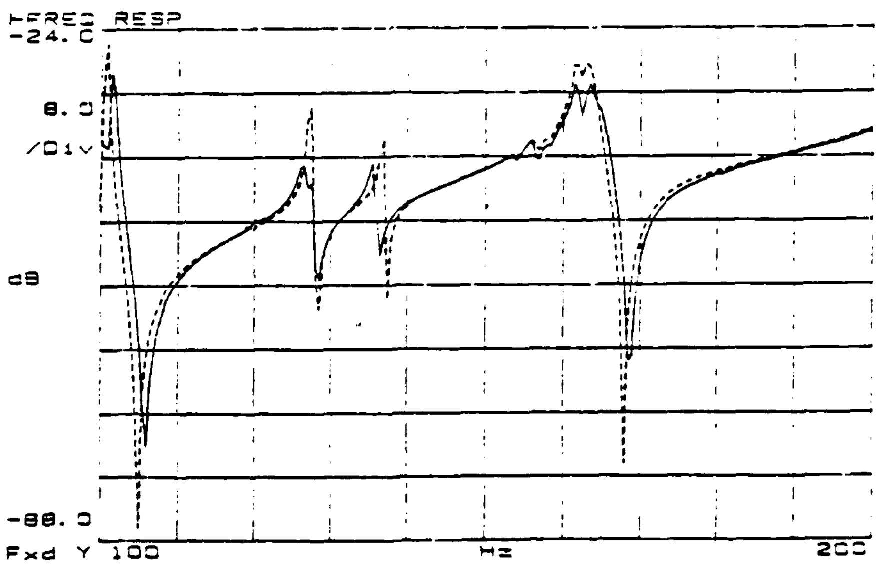

Figure 5.58 Frequency Response of the Viscoelastic Joint at 100% Torque.
(Dotted line is Non-Viscoelastic Joint)

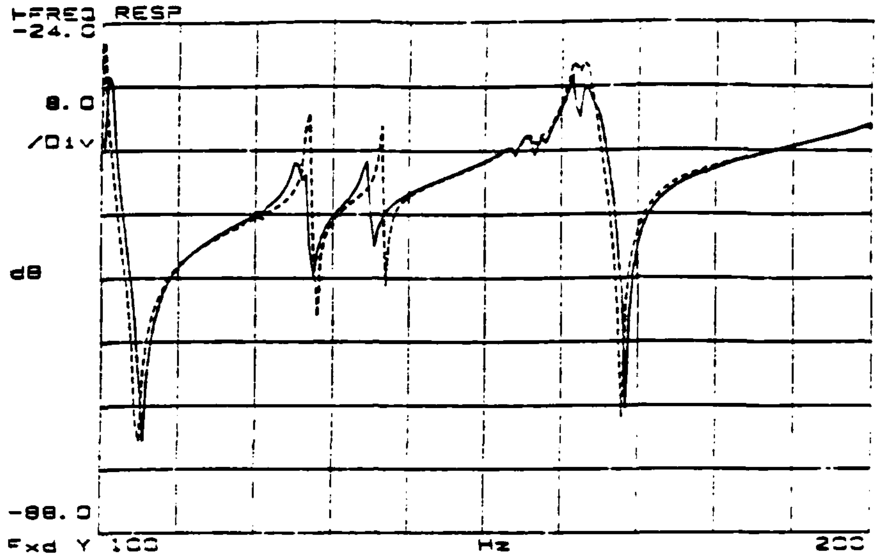

Figure 5.59 Frequency Response of the Viscoelastic Joint at 75% Torque.
(Dotted line is Non-Viscoelastic Joint)

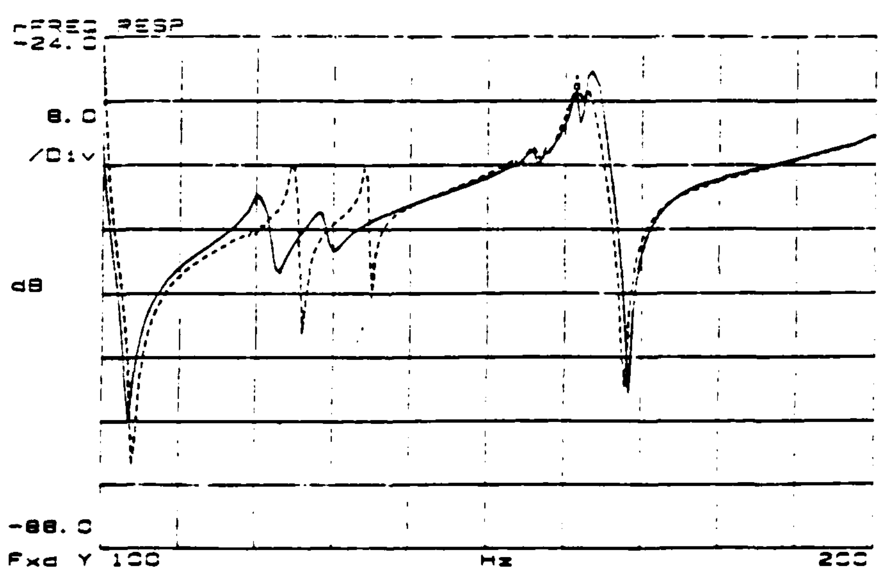

Figure 5.60 Frequency Response of the Viscoelastic Joint at 20% Torque.
(Dotted line is Non-Viscoelastic Joint)

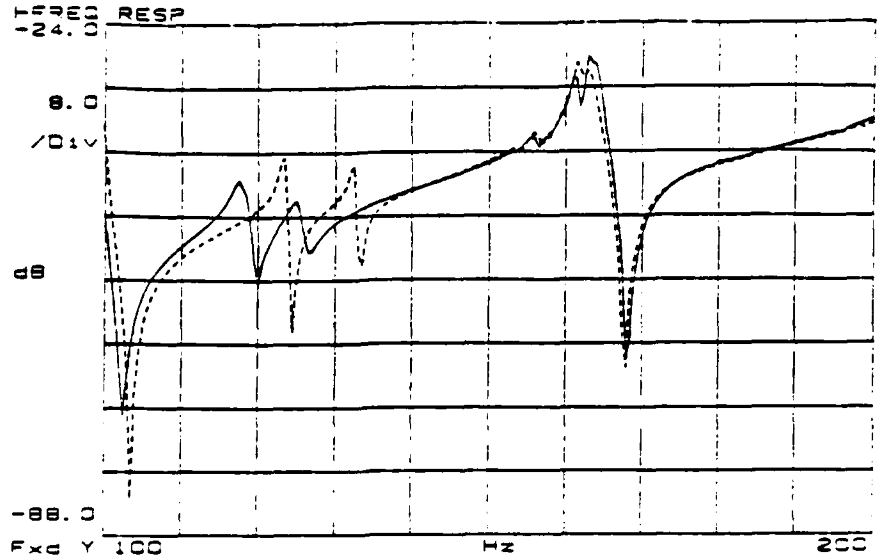

Figure 5.61 Frequency Response of the Viscoelastic Joint at 10% Torque.
(Dotted line is Non-Viscoelastic Joint)

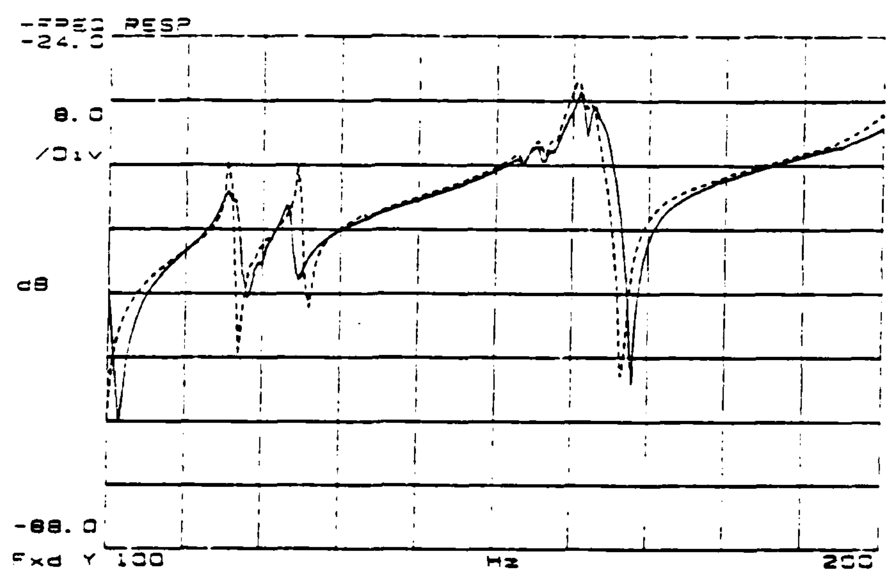

Figure 5.62 Frequency Response of the Viscoelastic Joint at 5% Torque.
(Dotted line is Non-Viscoelastic Joint)

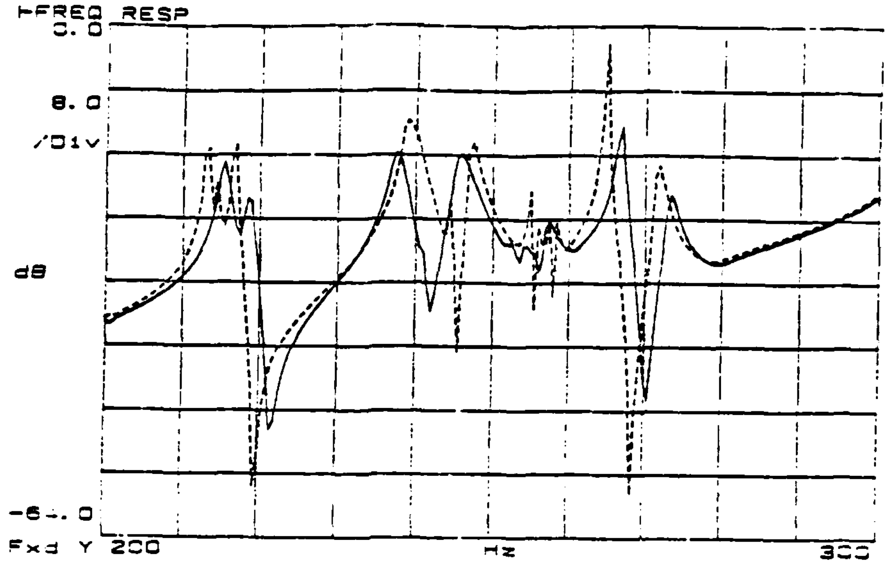

Figure 5.63 Frequency Response of the Viscoelastic Joint at 100% Torque.
(Dotted line is Non-Viscoelastic Joint)

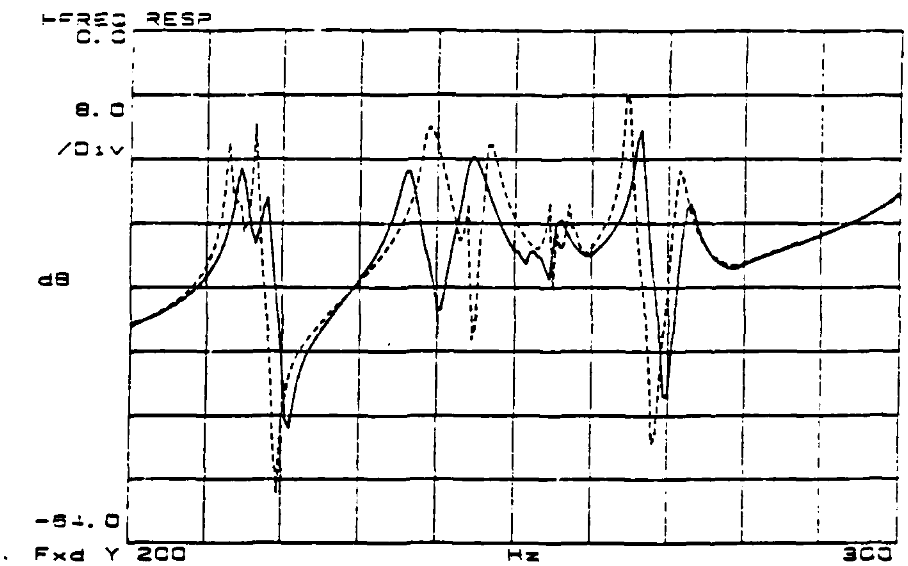

Figure 5.64 Frequency Response of the Viscoelastic Joint at 75% Torque.
(Dotted line is Non-Viscoelastic Joint)

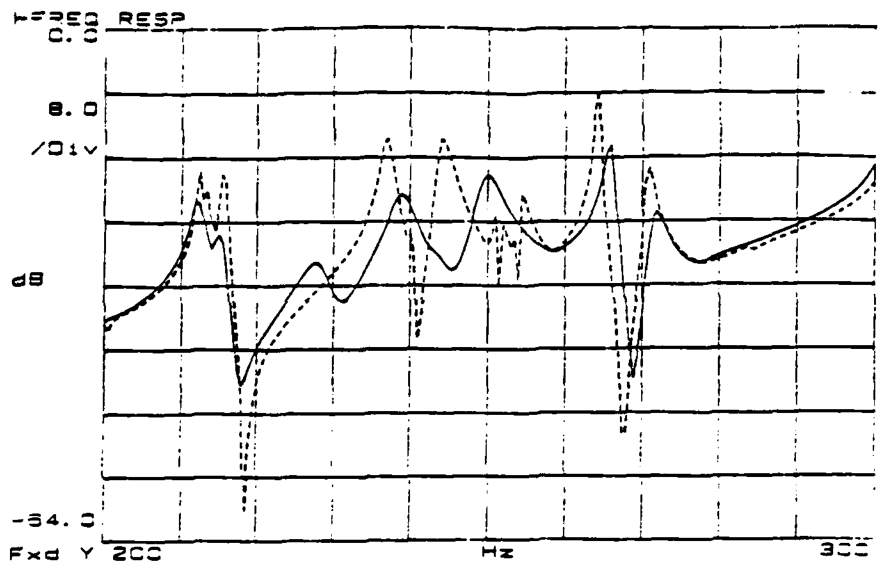

Figure 5.65 Frequency Response of the Viscoelastic Joint at 20% Torque.
(Dotted line is Non-Viscoelastic Joint)

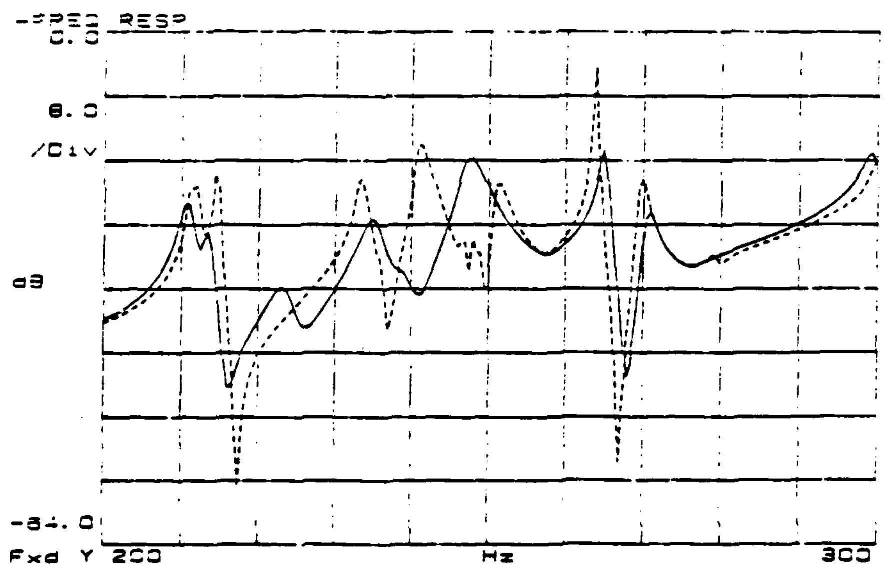

Figure 5.66 Frequency Response of the Viscoelastic Joint at 10% Torque.
(Dotted line is Non-Viscoelastic Joint)

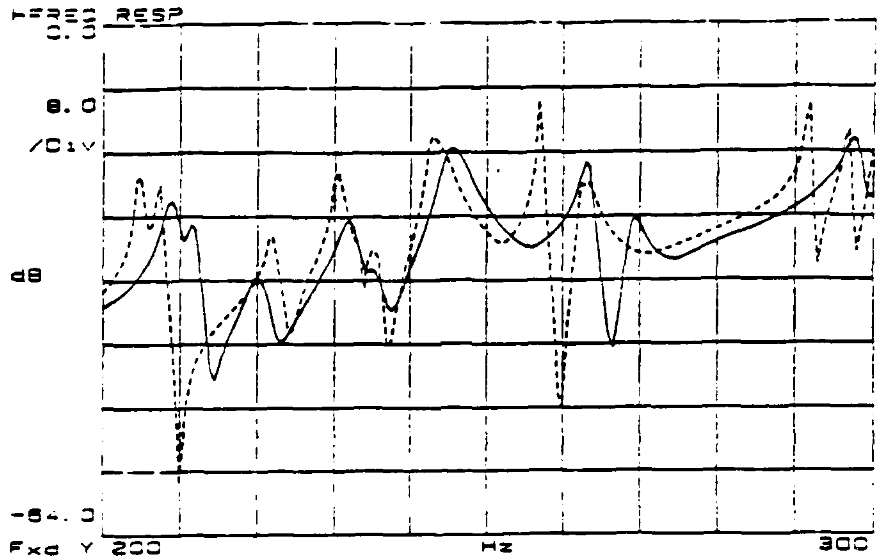

Figure 5.67 Frequency Response of the Viscoelastic Joint at 5% Torque. (Dotted line is Non-Viscoelastic Joint)

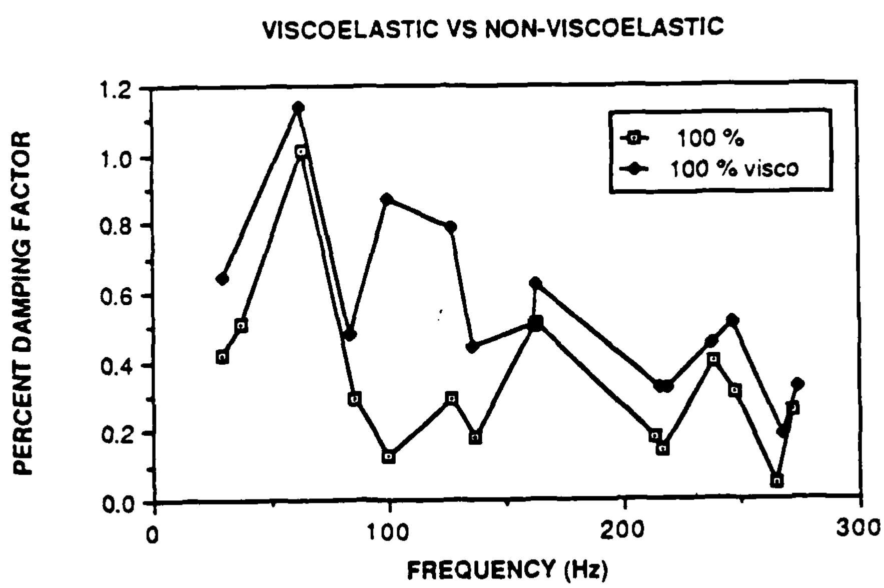

Figure 5.68 Percent Damping Factor for the Viscoelastic Joint vs the Non-Viscoelastic Joint at the same torque.

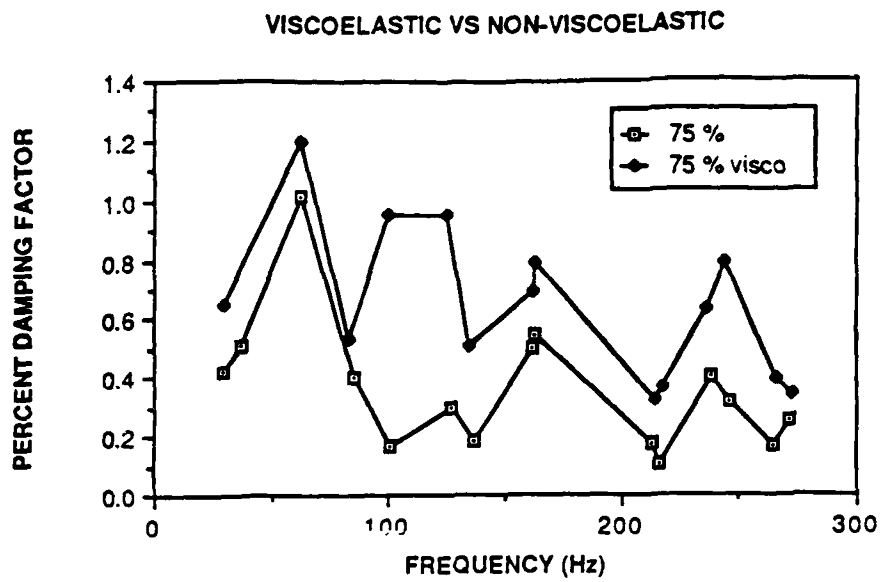

Figure 5.69 Percent Damping Factor for the Viscoelastic Joint vs the Non-Viscoelastic Joint at the same torque.

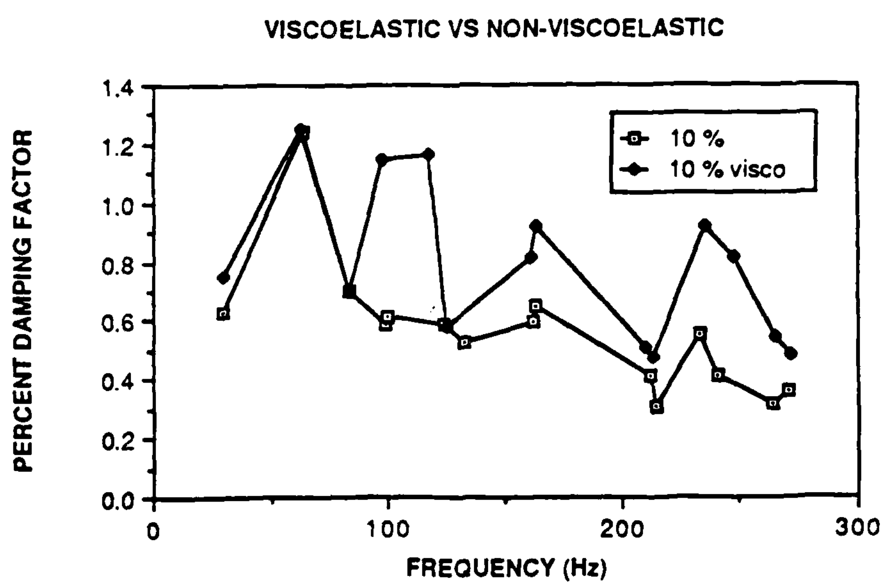

Figure 5.70 Percent Damping Factor for the Viscoelastic Joint vs the Non-Viscoelastic Joint at the same torque.

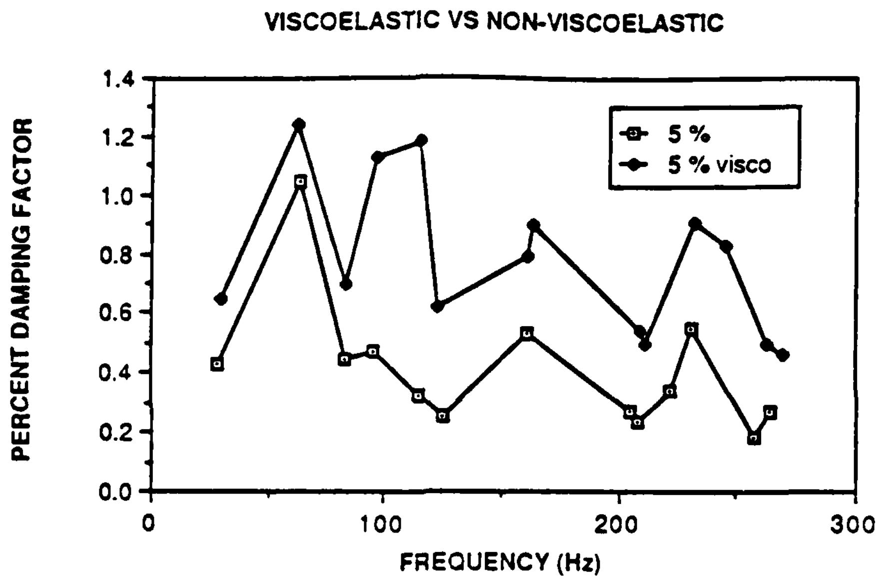

Figure 5.71 Percent Damping Factor for the Viscoelastic Joint vs the Non-Viscoelastic Joint at the same torque.

VI. CONCLUSION

The results for the varying contact force are similar to the study conducted on a single mode by Beards and Woodwat. They concluded that the damping of a single mode could be increased by varying the contact force associated with the joints. This study has indicated that the same phenomena occurs for a large number of modes of a complex structure. The damping increase is closely associated with mode shapes that provide relative motion at the joint interfaces. If the mode shape does not provide this, then the damping remains the same, unchanged from the varying of contact force. The increase damping does not come free. The maximum expected excitation force must be defined in order to ensure that the structure does not enter into the macroslip region since interstlcial friction will cause corrosion and possible loss of structural rigidity.

This study also indicates the possibility of tuning a structure by shifting undesirable resonance frequencies by varying the bolt torque. This also comes with some difficulties: there exists a possibility of adding a shifting resonance frequency to a resonance frequency that does not shift, or of obtaining an undesirable new resonance frequency with a larger amplitude than the original frequency response.

The addition of viscoelastic material at the joint is clearly an advantage that should be aggressively pursued. It provides equal or greater damping at all contact forces and also provides an additional friction force to maintain the structure in the microslip range. This material provides a greater frequency shift for

tuning, therefore providing the maximum shift attainable before macroslip can take place and friction corrosion occur.

The effects of an underwater environment were attempted, but the frequency responses obtain did not stabilized to a repeatable event. The amplitudes continued to decrease and resonance frequency shifted further down with increased time. This indicates the possibility of a wetting effect taking place at the joint interface. The joints in this model did not achieve total wetting after ten hours of soaking.

VII. RECOMMENDATIONS

The following are suggestions for further studies in this field:

1. Since this study utilized only one thickness of viscoelastic material the possibility of increasing the positive effect exists and should be investigated.
2. The possibility of the addition of two resonances frequencies must be examined closer under a more detailed study then the one conducted here.
3. A further investigation into the wetting of the joint mating surfaces, wetting time and extent of its overall effects on the structure could be research in detail.
4. The wetting effects on the viscoelastic material and the "bubbles" that are left at the mating surfaces lead to additional effects taking place at the joint interface.
5. The effect of protective coatings as well as addition of high damping material should be investigated to see if they could provide the same positive effects observed with the viscoelastic material.

LIST OF REFERENCES

1. Beards, C.F., and Woodwat, A., "The control of Frame Vibration by Friction Damping in Joints," J. of Vibration, Acous., Stress, and Reliability in Design, Vol. 107, Jan. 1985, pp. 26-32.

2. Den Hartog, J.P., "Forced Vibrations with Combined Coulomb and Viscous Friction," Trans. ASME, Vol. 53, APM-53-9,1931, pp. 107-115.

3. Pratt, T.K., and Williams, R., "Non-Linear Analysis of Stick/Slip Motion," J. of Sound and Vibration, Vol. 74, No. 4, 1981, pp. 531-542.

4. Caughey, T.K., "Sinusoidal Excitation of a System with Bilinear Hysteresis," J. of Applied Mech., Vol. 27, Dec. 1960, pp. 640-643.

5. Iwan, W.D., "Steady-State Dynamic Response of a Limited Slip System," J. of Applied Mech., Vol. 35, June 1968, pp. 322-326.

6. Muszynska, A., Jones, D.I.G., Lagnese, T., and Whitford, L., "On Non-Linear Response of Multiple Bladed Systems," Shock and Vibration Bull., Vol. 51, Part 3, May 1981, pp. 88-110.

7. Muszynska, A., and Jones, D.I.G., "A Parametric Study of Dynamic Response of a Discrete Model of Turbomachinery Bladed Disk," J. of Vibration, Acous., Stress, and Reliability in Design, Vol. 4, Oct. 1983, pp. 434-443.

8. Earles, S.W.E., and Philpot, M.G.,"Energy Dissipation at Plane Surface in Contact," J. of Mech. Engineering Science, Vol. 9, 1967, pp. 86-97.

9. Crawley, E.F., Sarver, G.L., and Mohr, D.G., "Experimental Measurement of Passive Material and Structural Damping for Flexible Space Structures," Acta Astronautica, Vol. 10, no. 5-6, 1983, pp. 381-393.

10. Menq, C.H., Bielak, J., and Griffin,J.H., "The Influence of Microslip on Vibratory Response, Part I: A New Microslip Model," J. of Sound and Vibration, Vol. 107, No. 2, 1986, pp. 279-293.

11. Menq, C.H., Bielak, J., and Griffin, J.H., "The Influence of Microslip on Vibratory Response, Part II: A Comparison with Experimental Results," J. of Sound and Vibration, Vol. 107, No. 2, 1986, pp. 295-307.

12. Beards, C.F., and Williams, J.L., "The Damping of Structural Vibration By Rotational Slip in Joints," J. of Sound and Vibration, Vol. 53, No. 3, 1977, pp. 333- 340.

13. Earles, S.W.E., and Williams, E.J., "A Linearized Analysis for Fictionally Damped Systems," J. of Sound and Vibration, Vol. 24, No. 4, 1972, pp. 445-458.

14. Srinivasan, A.V., and Cutts, D.G., "Dry Friction Damping Mechanisms in Engine Blades," J. of Engineering for Power, Vol. 105, April 1983, pp. 332-341.

15. Hewlett-Packard Company, "Fourier Analyzer Training Manual", Application Note 140-0.

16. Richardson M., "Modal Analysis Using Digital Test Systems," from the Seminar on Understanding Digital Control and Analysis in Vibration Test Systems, Shock and Vibration Information Center publication, May 1986.

17. Knouse, S.T., Effects of Boundary Conditions on the Damping Characteristics of a Randomly Excited Cast Nickel-Aluminum Bronze Specimen at Low Stress Levels M.S. Thesis, Naval Postgraduate School, Monterey, California, December 1984.

18. Milster, P.F., Effect of Temperature and Environmental Changes on the Damping Properties of Randomly Excited Metal Plate Specimens M.S. Thesis, Naval Postgraduate School, Monterey, California, September 1985.

19. Shin, Y.S., Kim, K., and Iverson, J.C., Analytical and Experimental Investigations of the Damping Characteristics of Bolted and Welded Structural Connections for Plates and Shells Progress Report, Naval Postgraduate School, Monterey, California, 1986.

INITIAL DISTRIBUTION LIST

		No. Copies
1.	Defense Technical Information Center Cameron Station Alexandria, Virginia 22304-6145	2
2.	Library, Code 0142 Naval Postgraduate School Monterey, California 93943-5002	2
3.	Dean of Science and Engineering, Code 06 Naval Postgraduate School Monterey, California 93943-5000	2
4.	Research Administrations Office, Code 012 Naval Postgraduate School Monterey, California 93943-5000	1
5.	Department Chairman, Code 69 Department of Mechanical Engineering Naval Postgraduate School Monterey, California 93943-5000	1
6.	Professor Y.S. Shin, Code 69Sg Department of Mechanical Engineering Naval Postgraduate School Monterey, California 93943-5000	3
7.	Dr. K. Kim, Code 69Ki Department of Mechanical Engineering Naval Postgraduate School Monterey, California 93943-5000	1
8.	Dr. Arthur Kilcullen, Code 1962 David W. Taylor Naval Ship R&D Center Bethesda, Maryland 20084	5
9.	Mrs. Kathy Wong, Code 2812 David W. Taylor Naval Ship R&D Center Annapolis, Maryland 21402	1
10.	Mr. Robert Hardy, Code 2803 David W. Taylor Naval Ship R&D Center Annapolis, Maryland 21402	1

11. Dr. D.J. Vendittis, Code 196 1
David W. Taylor Naval Ship R&D Center
Ship Acoustics Department (196)
Bethesda, Maryland 20084

12. Mr. V.J. Castelli, Code 2844 1
David W. Taylor Naval Ship R&D Center
Annapolis, Maryland 21402

13. Professor Perkins, Code 69Ps 1
Department of Mechanical Engineering
Naval Postgraduate School
Monterey, California 93943-5000

14. Dr. B. Whang, Code 1750.2 1
David W. Taylor Naval Ship R&D Center
Hull Group Head, Submarine Protection Div.
Bethesda, Maryland 20084

15. Dr. N. T. Tsai 1
Defense Nuclear Agency
SPSS
Washington, D.C. 20305-1000

16. Mr. Jonathan Iverson 3
404 Brandywine Lane
Pleasant Hill, California 94523

END
DATE
FILMED
JAN
1988